Physica D 389 (2019) 24–50

Contents lists available at ScienceDirect

Physica D

journal homepage: www.elsevier.com/locate/physd

Strictly supersonic solitary waves in lattices with second-neighbor interactions

Lev Truskinovsky [a], Anna Vainchtein [b,*]

[a] PMMH, CNRS-UMR 7636, ESPCI ParisTech, 10 Rue Vauquelin, Paris, 75005, France
[b] Department of Mathematics, University of Pittsburgh, Pittsburgh, PA 15260, USA

HIGHLIGHTS

- Solitary waves in chains with competing interactions were studied analytically.
- Some obtained solutions are of envelope type and involve two length scales.
- There is a parameter range where solitary waves are strictly supersonic.
- Higher-order quasicontinuum theories are necessary to capture these effects.

ARTICLE INFO

Article history:
Received 29 March 2018
Received in revised form 13 September 2018
Accepted 2 October 2018
Available online 12 October 2018
Communicated by D. Pelinovsky

Keywords:
Nonlinear lattice
Solitary waves
Second-neighbor interactions
Quasicontinuum model
Modulation equation

ABSTRACT

We consider a monatomic nonlinear mass–spring chain with first and second-neighbor interactions and show that there is a parameter range where solitary waves in this system are *strictly supersonic*. In these regimes standard quasicontinuum theories, targeting long-wave limits of lattice models, are not adequate since even weak strictly supersonic solitary waves are of envelope type and crucially involve a microscopic scale in addition to the mesoscopic scale of the envelope. To capture this effect in a continuum setting it is necessary to employ unconventional, higher-order quasicontinuum approximations carrying more than one length scale.

1. Introduction

Manipulation of mechanical waves with lattice scales opens enormous possibilities in mechanical signal transmission. Nonlinearity plays an important role in such processes because at finite amplitudes the underlying mechanical systems can access regimes that allow nontrivial energy redistribution among different scales. For instance, even the simplest nonlinear mass–spring chains exhibit spectral localization of energy, resulting in the formation of dynamic coherent structures. In applications, it is desirable to control the propagation velocities of such structures by fine-tuning particle interactions [1].

An important role in the design of the coherent energy transport in nonlinear lattices is played by acoustic solitary waves, nontopological collective excitations which propagate without distortion and can be therefore used to transmit information. Acoustic solitary waves in the simplest one-dimensional lattices with nearest-neighbor (NN) interactions are described by the Fermi–Pasta–Ulam (FPU) model [2]. It was shown that these waves are necessarily *supersonic* with respect to the unstrained state ahead of them, and their existence was proved rigorously for interaction potentials with superquadratic growth at infinity [3]. Near the sonic limit such waves become weak and delocalized and are therefore adequately captured by quasicontinuum theories of KdV type that involve a single internal length scale [4,5]. Rather remarkably, we show that the addition of *linear* next-to-nearest neighbor (NNN) interactions to the FPU model can change this picture qualitatively.

More specifically, we show that if NN and NNN interactions *compete* in the sense that NN interactions are stabilizing while the NNN interactions are destabilizing, there is a range of parameters where the weakest solitary waves, that are necessarily supersonic, disassociate from the solutions of the linearized continuum (homogenized) equations, that are necessarily sonic. In other words, there is a finite gap where supersonic solitary waves do not exist.

* Corresponding author.
E-mail address: aav4@pitt.edu (A. Vainchtein).

https://doi.org/10.1016/j.physd.2018.10.001
0167-2789/

Supersonic solitary waves in these regimes that are closest to the gap have an envelope-type oscillatory structure and are characterized by two length scales: one microscopic and another one mesoscopic. Such regimes exist when NN and NNN interactions are sufficiently antagonistic and therefore of non-perturbative nature. To capture such strongly discrete effects in a continuum setting, KdV-type approximations relying on a single mesoscopic length scale, are not sufficient and one is led to consider 'post-KdV' quasicontinuum approximations incorporating more than one internal length scale.

Interestingly, not only the existence of *strictly supersonic* solitary waves was missed in the previous studies of the FPU problem with competing NNN interactions, but also the proposed low-order KdV-type quasicontinuum approximations suggested a qualitatively new effect: the existence of *subsonic* solitary waves that are prohibited in the NN model [6–8]. Here we argue that this is an artifact of the approximation by showing that subsonic propagation of solitary waves cannot be generic in the discrete model due to the presence of radiative (non-decaying) modes at subsonic velocities. Moreover, we show that quasicontinuum approximations of sufficiently high order, adequately capturing the velocity gap between the linear waves in the naive homogenized theory and the slowest solitary waves in the discrete theory, also exclude subsonic propagation of solitary waves.

The necessity of using higher-order continuum theories to describe NNN chains with competing interactions was probably first realized by Mindlin [9] who studied the linearized elastostatics of such lattices and came across the regimes where the characteristic eigenvalue is complex and is therefore characterized by two length scales. His conclusion was that the adequate quasicontinuum description in this case must necessarily include both first and second gradients of strain; for more recent results in this direction, see [10–12]. The need to use two spatial scales in the averaged description was also realized in the studies of capillary–gravity water waves where the dispersion relation has some features similar to the one in NNN lattices. In this context, weak two-scale envelope-type solitary waves were also identified [13,14], and it was shown that their amplitude can be described by a nonlinear Schrödinger (NLS) equation augmented by higher-order terms [15,16].

To obtain explicit solutions of the discrete problem, we use a model with piecewise quadratic NN and quadratic NNN interaction energies. The idea to confine nonlinearity to a single point was used in [17] to study the solitary waves in the FPU system; see also [18–23] for a similar approach in studies of dislocations, cracks and phase boundaries. The family of exact solutions obtained in [17] was broad enough to cover the whole spectrum of behaviors from quasicontinuum to anticontinuum. Here we extend this class of solutions to systems with additional linear NNN interactions.

Of a particular interest for us are the envelope discrete solitary waves which bifurcate from the solutions of the linearized equations with a finite wave length at the point on the dispersion curve where group and phase velocities coincide. We emphasize that these are genuine traveling waves, as opposed to envelope-type discrete breathers that also exist in lattices with second-neighbor interactions [6]. To demonstrate that the bifurcating strictly supersonic solitary waves are not an artifact of the piecewise quadratic nonlinearity, we consider the case of smooth NN interactions strongly competing with linear NNN bonds and derive the corresponding higher-order NLS amplitude modulation equation, which yields a leading-order approximation of the bifurcating solution. Using this approximation as an initial seed, we then numerically construct the bifurcating branch of solitary waves. Our numerical simulations validate the existence of strictly supersonic solitary waves in the NNN models with general nonlinearity and suggest their stable propagation.

Since the discrete theory is analytically opaque in the general case, the natural step is to develop adequate quasicontinuum approximations amenable to analytical studies. After demonstrating that the low-order quasicontinuum theories fail to capture the envelope-type solitary waves, we turn to a higher-order continuum approximation based on a fourth-order Taylor expansion of the discrete operator in the traveling wave equation and show that it is compatible with this effect. In the case of piecewise linear NN interactions we compare this theory and the low-order truncation of the discrete solution, which relies only on the first four roots of the characteristic equation in each linear regime that are closest to the origin, with the full solution of the discrete problem. The comparison identifies a parameter regime where both approximations adequately capture the discrete problem.

The paper is organized as follows. In Section 2 we introduce the discrete model, study the dispersion relation for the linearized problem and establish the existence of the velocity gap discussed in the Introduction. In Section 3 we specialize the model to the case of piecewise linear NNN interactions. We then use a Wiener–Hopf-type approach to obtain in Section 4 a one-parameter family of explicit solitary wave solution of this model in the form of infinite series. In Section 5 we give a simple illustration of this general class of solutions by considering the simplest truncation of the infinite series. The stability of the generic solitary waves in this model is studied numerically in Section 6. We proceed in Section 7 by developing a higher-order quasicontinuum approximation and comparing it to the discrete problem in the analytically tractable case of piecewise linear NN interactions. The case of a general smooth NN potential is considered in Section 8, where we construct a higher-order NLS modulation equation and use it to study the bifurcation of the strictly supersonic solitary waves. Section 9 contains our conclusions. Some technical results are presented in the form of Appendices.

2. The model

Consider an infinite chain of interacting point masses. In dimensionless variables the energy (Hamiltonian) of the system is given by

$$\mathcal{H} = \sum_{n=-\infty}^{\infty} \left[\frac{1}{2}\dot{u}_n^2 + \phi(u_n - u_{n-1}) + \frac{\beta}{8}(u_n - u_{n-2})^2 \right]. \tag{1}$$

Here $u_n(t)$ is the displacement of the nth mass at the time t, $\dot{u}_n = u_n'(t)$, and $\phi(w)$ is a potential governing anharmonic interactions between the nearest (first) neighbors. In what follows we assume that it satisfies $\phi(0) = \phi'(0) = 0$, is locally convex ($\phi''(w) > 0$) in an open interval containing zero, where it has a minimum, and rescaled so that $\phi''(0) = 1$. The last term in (1) corresponds to harmonic interactions between the next-to-nearest (second) neighbors. The relative strength of second-neighbor interactions is measured by the constant coefficient β; $\beta = 0$ corresponds to the classical case of the FPU lattice with only first-neighbor interactions.

The dynamics of the system is governed by the following system of ordinary differential equations:

$$\ddot{u}_n = f(u_{n+1} - u_n) - f(u_n - u_{n-1}) + \frac{\beta}{4}(u_{n+2} - 2u_n + u_{n-2}), \tag{2}$$

where $f(w) = \phi'(w)$ is the anharmonic interaction force. By the above assumptions, $f(0) = 0$, $f'(0) = 1$ and $f'(w) > 0$ near $w = 0$. The macroscopic stress in the chain is given by $\Sigma(w) = f(w) + \beta w$, with the elastic modulus $\Sigma'(0) = 1 + \beta$. We note that for stability of the undeformed state of the chain it is necessary and sufficient that $\beta > -1$ (e.g. [24]). Behind this lower stability bound is the fact that for $\beta < 0$, NN and NNN interactions are *competing*. Indeed, while the NN interaction potential $\phi(w)$ is convex near the

undeformed state and thus favors states with homogeneous strain, the NNN potential is concave, favoring instead fine-scale oscillations [25,10,26,27]. The combination of these two interactions can support homogeneous states only if NNN interactions are not too strong, which leads to the condition $\beta > -1$. As we show below (see also [6–8]), competing interactions generate qualitatively new effects in solitary wave dynamics compared to the case $\beta \geq 0$.

It will be convenient to rewrite (2) in terms of strain variables

$$w_n = u_n - u_{n-1}.$$

This yields

$$\ddot{w}_n = f(w_{n+1}) - 2f(w_n) + f(w_{n-1}) + \frac{\beta}{4}(w_{n+2} - 2w_n + w_{n-2}). \quad (3)$$

Solitary waves are spatially localized traveling wave solutions of (3). Substituting the traveling wave ansatz

$$w_n(t) = w(x), \quad x = n - Vt,$$

where V is the velocity of the wave, in (3) yields the advance-delay differential equation

$$V^2 w'' = f(w(x+1)) - 2f(w(x)) + f(w(x-1)) + \frac{\beta}{4}(w(x+2) - 2w(x) + w(x-2)). \quad (4)$$

Solitary wave solutions correspond to homoclinic trajectories of (4) selected by the following conditions at infinity:

$$w(x) \to 0 \quad \text{as } |x| \to \infty. \quad (5)$$

Suppose that (4) has a solitary wave solution $w(x)$ for given V, $f(w)$ and β. Its asymptotic behavior at infinity is then given by

$$w(x) \sim \mathcal{B}e^{ikx} + \bar{\mathcal{B}}e^{-i\bar{k}x}, \quad x \to \infty, \quad (6)$$

where $\mathcal{B}$ and k are complex constants, and $\mathrm{Im}k > 0$ to ensure the decay to zero. Linearizing (4) about $w = 0$, one can see that k must be a nonzero root of $L(k) = 0$, where

$$L(k) = 4\sin^2\frac{k}{2} + \beta\sin^2 k - V^2k^2 \quad (7)$$

is the characteristic function for the zero-strain state. Clearly, $L(k) = \omega^2(k) - V^2k^2$, where

$$\omega^2 = 4\sin^2\frac{k}{2} + \beta\sin^2 k \quad (8)$$

is the corresponding dispersion relation. The structure of the nonzero roots of (7) for different values of β is illustrated in Fig. 1.

Note that if k is a root of $L(k) = 0$, then so are $\bar{k}$, $-k$ and $-\bar{k}$, so the complex roots always exist in quadruples. As a consequence, the real roots are symmetric about the imaginary axis and the imaginary roots are symmetric about the real axis. The complex roots form in $(\mathrm{Re}k, \mathrm{Im}k, V)$ space two sets of branches. One set (shown in green in Fig. 1) bifurcate from the maxima of real and purely imaginary roots. Another set (shown in red in Fig. 1) emanate from $(V, k) = (0, \pm\pi \pm 2i\mathrm{arcsinh}(1/\sqrt{\beta}) \pm 2\pi j)$ for $\beta > 0$ and from $(V, k) = (0, \pm 2i\mathrm{arccosh}(1/\sqrt{-\beta}) \pm 2\pi j)$ for $\beta < 0$, where j is any nonnegative integer, and these branches approach infinity when $\beta \to 0$. The structure of the red branches becomes more complex at large enough positive β, when some of the branches split at certain bifurcation velocity values and become attached to additional maxima and minima acquired by the real root curve. However, this parameter range will not be of interest for the construction of solitary waves.

We now observe that solitary waves are generally incompatible with the existence of the nonzero real roots in (6), which in a generic situation lead to non-decaying oscillations (radiation) at infinity. For $\beta \geq -1/4$, such roots exist for $0 \leq V < c$, where

$$c = \sqrt{1+\beta} \quad (9)$$

is the speed of sound and the maximal phase velocity for linear waves in this β range, corresponding to the wave number $k = 0$ ($c = \omega'(0)$). Therefore, solitary waves must be *supersonic*, $V > c$, in this parameter regime. For $-1 < \beta < -1/4$, the nonzero real roots exist for $0 \leq V \leq V_{\mathrm{m}}(\beta)$, where $V_{\mathrm{m}} > c$ is the β-dependent maximum of the real root branch, as illustrated in Figs. 1(d) and 2(b):

$$V_{\mathrm{m}} = \max\left\{\frac{\omega(k)}{k} : k \in \mathbb{R},\ k > 0,\ -1 < \beta < -1/4\right\}. \quad (10)$$

This maximal phase velocity corresponds to the wave number $k = k_{\mathrm{m}} > 0$ at which the phase and group velocities coincide:

$$\omega'(k_{\mathrm{m}}) = \omega(k_{\mathrm{m}})/k_{\mathrm{m}} = V_{\mathrm{m}}. \quad (11)$$

Hence in this case solitary waves are necessarily *strictly supersonic*, $V > V_{\mathrm{m}}$, and there is a finite *velocity gap* between V_{m} and c. At $\beta = -1/4$, the gap closes because $V_{\mathrm{m}} = c$. The velocity range where solitary waves may exist at a given β is thus given by

$$\begin{aligned} &V > c, \quad \beta \geq -1/4 \quad \text{and} \\ &V > V_{\mathrm{m}} > c, \quad -1 < \beta < -1/4, \end{aligned} \quad (12)$$

as illustrated in Fig. 2(b). As discussed above, (12) means that V must be above the maximal phase velocity for linear waves.

We now focus on the nature of the asymptotic behavior of the solutions (6) of the linearized equations at infinity; see also [8]. The principal term in the asymptotic limit is determined by the nonzero root of $L(k) = 0$ with the smallest magnitude, given that $\mathrm{Im}k > 0$. For $\beta \geq 0$, $V > c$, we have $k = iq$, $q > 0$, which implies that potential solitary wave must have a monotone decay with the length scale $l = 1/q$. As the sonic limit is approached, q tends to zero and one can expect the KdV-type delocalization of the solitary wave.

When $-1/4 < \beta < 0$, the purely imaginary roots have a finite maximal velocity

$$V_{\mathrm{cr}} = \max\{V > 0 : L(iq) = 0,\ q \in \mathbb{R},\ q > 0, \ -1/4 < \beta < 0\}, \quad (13)$$

which is above the sound speed, as illustrated in Fig. 1(c). For $c < V < V_{\mathrm{cr}}(\beta)$, the equation $L(k) = 0$ has two imaginary roots in the upper half plane, iq_1 and iq_2, $q_2 > q_1 > 0$, which define two length scales, $l_1 = 1/q_1$ and $l_2 = 1/q_2 < l_1$. In this case the behavior at infinity must be monotone and dominated by the larger length scale l_1. In the sonic limit, q_1 tends to zero, so $l_1 \to \infty$, and we expect solitary waves to delocalize as in the case $\beta \geq 0$. At $V = V_{\mathrm{cr}}(\beta)$ the two roots merge into one, producing at $V > V_{\mathrm{cr}}$ two complex roots $k = \pm\xi + i\eta$, $\xi > 0$, $\eta > 0$. This implies that solitary waves in this range exhibit *oscillatory decay* with the two length scales $1/\xi$ and $1/\eta$ governing the frequency and the amplitude decay of the oscillations, respectively. The transition from monotone to oscillatory decay was also discussed in [8]. As β approaches zero from below, $V_{\mathrm{cr}} \to \infty$, while at $\beta = -1/4$ we have $V_{\mathrm{cr}} = V_{\mathrm{m}} = c$. The curve $V_{\mathrm{cr}}(\beta)$ is shown in Fig. 2(b) by a dashed line.

Finally, at $-1 < \beta < -1/4$, when solitary waves must be strictly supersonic, $V > V_{\mathrm{m}} > c$, the nonzero roots of $L(k) = 0$ with the smallest magnitude are complex, and therefore the decay is again oscillatory. As the lower velocity bound V_{m} is approached, the imaginary part η of the root k tends to zero while the magnitude ξ of the real part tends to the finite positive limit k_{m} defined in (11). This suggests that the near-gap solitary waves must be in the form of slowly modulated short-scale oscillations. Such *essentially*

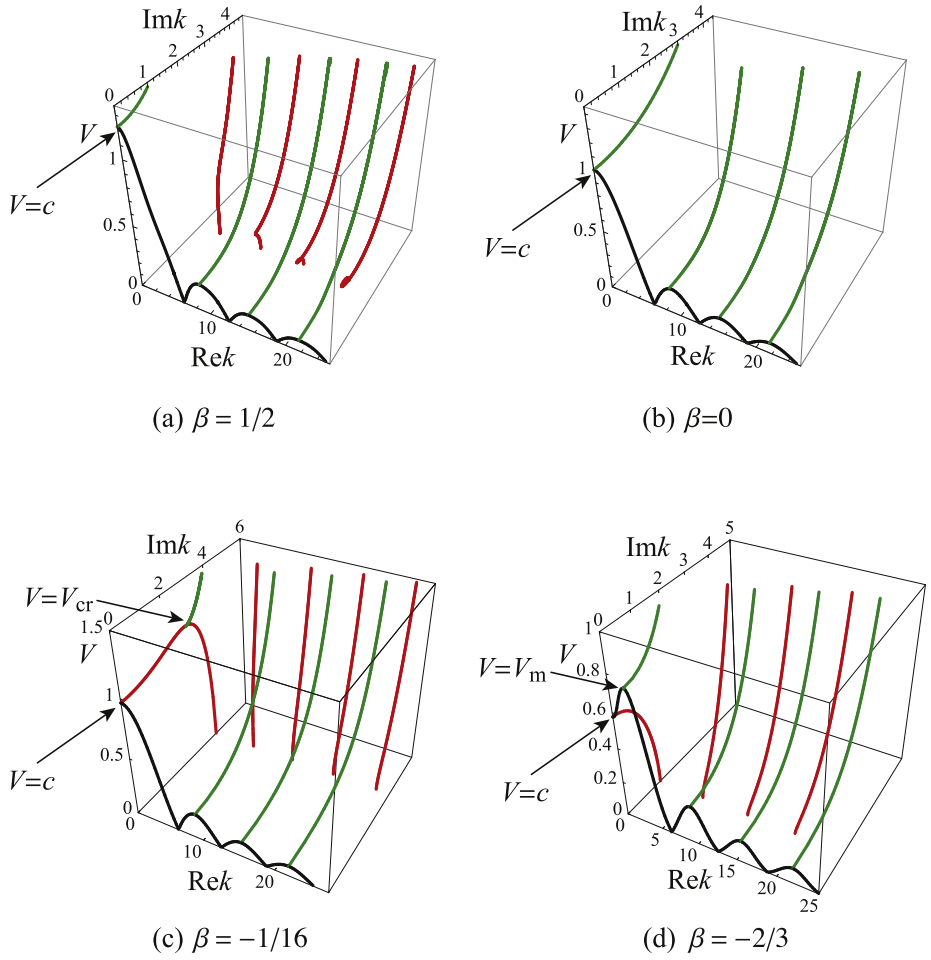

Fig. 1. Representative structure of nonzero roots of $L(k) = 0$ at $V \geq 0$ and (a) small $\beta > 0$; (b) $\beta = 0$; (c) $-1/4 < \beta < 0$; (d) $-1 < \beta < -1/4$. Due to the symmetry of the roots about the real and imaginary axes, only roots in the first quadrant are shown. The root branches continue to infinity. At $\beta = -1/4$ the critical velocities c, $V_{\rm cr}$ and $V_{\rm m}$ coincide.

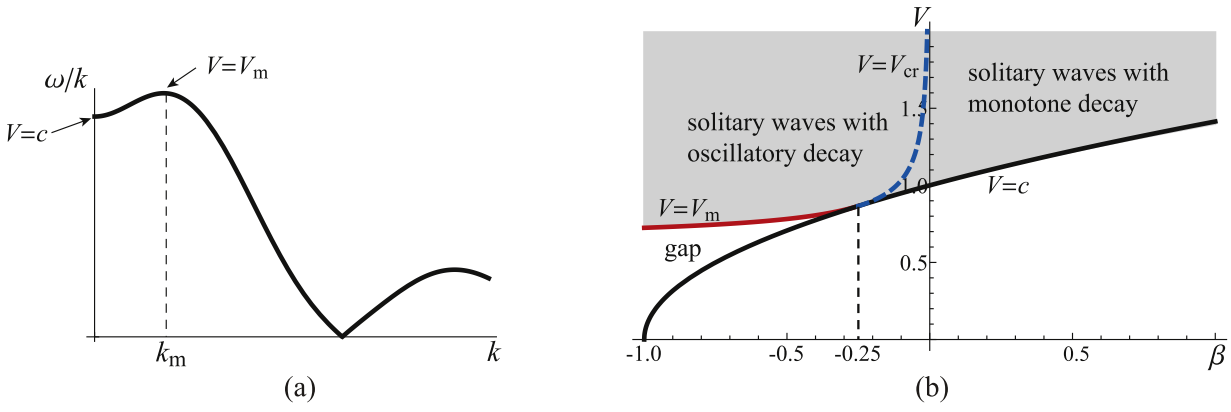

Fig. 2. (a) Typical dispersion curve for the phase velocity at $-1 < \beta < -1/4$, with a maximum $V_{\rm m} > c$ at $k = k_{\rm m}$. Solitary waves bifurcate from the maximum point and have velocities $V > V_{\rm m}$. (b) The domain (shaded region) in (β, V) plane where solitary waves may exist according to (12). See the text for details.

discrete behavior of solutions is clearly out of reach for the KdV equation describing similar weak solitary waves in the interval $\beta \geq -1/4$. We note that in view of (58) below, the interval $-1 < \beta < -1/4$ is the most widely used range of β values in various applications because only in this interval the standard gradient expansion of the elastic energy leads to a well defined continuum theory.

3. Piecewise linear NN interactions

To further investigate the discrete model (4) we now introduce NN interactions for which exact solitary wave solutions can be constructed. We limit our attention to the case of competitive second-neighbor interactions, with $-1 < \beta < 0$, since our analysis above and the earlier work [8,6,7] show that this is the parameter range

where the second-neighbor interactions introduce new features, while the case $\beta > 0$ is qualitatively similar to the case $\beta = 0$.

Consider a convex biquadratic potential $\phi(w)$ giving rise to continuous piecewise linear interaction force between the nearest neighbors in the form:

$$f(w) = \begin{cases} w, & w \le w_c \\ \alpha(w - w_c) + w_c, & w \ge w_c. \end{cases} \tag{14}$$

Here the parameter α is the ratio of the elastic moduli in the two linear regimes separated by the critical strain w_c. We consider the case $\alpha > 1$, corresponding to the hardening nonlinearity. The dimensionless sound speeds associated with the first and second linear regimes are

$$c_1 = \sqrt{1+\beta}, \quad c_2 = \sqrt{\alpha+\beta}. \tag{15}$$

Under our assumptions $c_1 < c_2$. The limiting case $\beta = 0$ was studied in [17].

Assume that solitary wave solution takes values in the second linear segment ($w(x) > w_c$) when $|x| < z$, for some $z > 0$ to be determined. We further assume that for $|x| > z$, $w(x) < w_c$ (first linear segment) and that $w(\pm z) = w_c$. Due to the linear nature of the problem in $|x| > z$ and $|x| < z$, the solution can be written in terms of plane waves with wave numbers satisfying the characteristic equations $L(k) = 0$ and $G(k) = 0$, respectively. Here $L(k)$, given by (7), and

$$G(k) = 4\alpha \sin^2\frac{k}{2} + \beta \sin^2 k - V^2 k^2 \tag{16}$$

are the Fourier images of the corresponding linear advance-delay differential operators. Both functions have a double zero at $k = 0$, while the structure of their nonzero roots is shown in Fig. 1, where for $L(k) = 0$ we have $c = c_1$, while for $G(k) = 0$ we need to replace β by β/α and V by $V/\sqrt{\alpha}$ and set $c = c_2/\sqrt{\alpha}$. Real and imaginary roots at $-1 < \beta < 0$ are shown in Fig. 3. Note that $G(k) = 0$ always has real roots for velocities below c_2. We recall that all roots are symmetric about the real and imaginary axes.

We now determine the velocity range where solitary waves may exist. As we have already discussed, for existence of solitary waves it is necessary that $L(k) = 0$ has no nonzero real roots but has roots with $\mathrm{Im} k > 0$. In order for a homoclinic connection involving the second linear regime to exist it is also necessary that $V < c_2$. Together this yields the velocity intervals

$$\begin{aligned} &c_1 < V < c_2, \quad \beta \ge -1/4 \quad \text{and} \\ &V_{\mathrm{m}} < V < c_2, \quad -1 < \beta < -1/4, \end{aligned} \tag{17}$$

which are shown by shaded regions in Fig. 3. Here we recall that V_{m} is the maximal phase velocity defined in (10). For $-1 < \beta < 0$, the solitary wave solution in the corresponding velocity intervals is an even function of x that has the form

$$w(x) = \begin{cases} a_0 + \sum_{j=1}^{\infty} a_j \cos(\gamma_j x), & |x| \le z \\ \sum_{j=1}^{\infty} b_j \exp(i\lambda_j^+ |x|), & |x| \ge z. \end{cases} \tag{18}$$

Here γ_j are the roots of $G(\gamma) = 0$ that have either positive real part, $\mathrm{Re}(\gamma_j) > 0$, or are purely imaginary and belong to the upper half-plane, $\mathrm{Re}(\gamma_j) = 0$, $\mathrm{Im}(\gamma_j) > 0$, while λ_j^+ are the roots of $L(\lambda) = 0$ with positive imaginary part, $\mathrm{Im}(\lambda_j^+) > 0$. As described in the next section, the infinite set of coefficients a_j and b_j and the value of z can be found by solving a linear integral differential equation and a nonlinear eigenvalue problem associated with it.

4. Solution of the discrete problem

To construct the solitary wave solutions, we use the approach developed in [17] (see also [28–30], where a similar method was used to obtain heteroclinic traveling waves describing dislocations and phase boundaries).

Recall that under our assumptions $f(w(x)) = w(x)$ outside the core region, at $|x| > z$, where $w(x) < w_c$. This condition can be written in the form

$$f(w(x)) = w(x) + \mathcal{A}\int_{-z}^{z} \theta(s - x) h(s) ds, \tag{19}$$

where $\theta(x)$ is the unit step function ($\theta(x) = 1$ for $x > 0$, $\theta(x) = 0$ for $x < 0$), $\mathcal{A} > 0$ is a constant to be determined, and $h(x)$ is an unknown odd shape function, $h(-x) = -h(x)$, satisfying $h(s) \equiv 0$ for $|s| > z$ and normalized so that

$$\int_0^z h(s) ds = 1. \tag{20}$$

Indeed, observe that $\theta(s-x) = 0$ when $x > z$ and $\theta(s-x) = 1$ when $x < -z$ for all $|s| \le z$, so the integral in (19) is zero in both cases (in the latter case because $h(x)$ is odd), yielding $f(w(x)) = w(x)$ for $|x| > z$. Meanwhile, for $|x| < z$, where $w(x) > w_c$, we use (19) and (14) to obtain $f(w(x)) = w(x) + \mathcal{A}\int_x^z h(s) ds = \alpha(w(x) - w_c) + w_c$. This yields the following relation between the shape function $h(x)$ and the odd derivative $w'(x)$ of the solution in the core region:

$$w'(x) = \frac{\mathcal{A}}{1-\alpha} h(x), \quad |x| < z. \tag{21}$$

Suppose now that the function $h(x)$ is known. Substituting the ansatz (19) into (4) and solving the corresponding linear problem, we obtain

$$w(x) = \frac{\mathcal{A}}{2\pi i(\alpha - 1)} \int_{-\infty}^{\infty} \left(\frac{G(k)}{L(k)} - 1\right) \frac{H(k)}{k} e^{ikx} dk, \tag{22}$$

where $H(k) = \int_{-z}^{z} h(s) \exp(-iks) ds$ is the Fourier transform of $h(s)$. Using (21) and (22), we then find that the shape function must be a nontrivial solution of the convolution-type Fredholm integral equation of second kind:

$$(\alpha - 1)\int_{-z}^{z} \mathcal{Q}(x - s) h(s) ds + h(x) = 0, \quad |x| < z, \tag{23}$$

where we introduced the V-dependent kernel

$$\mathcal{Q}(x) = \frac{1}{2\pi(\alpha - 1)} \int_{-\infty}^{\infty} \left(\frac{G(k)}{L(k)} - 1\right) e^{ikx} dk, \tag{24}$$

which is an even function. The linear part of the problem thus reduces to finding a nontrivial solution of the homogeneous Fredholm integral equation of second kind for $h(x)$. Such solutions only exist if the linear operator in the left hand side of (23) has a zero eigenvalue. The condition for the existence of the zero eigenvalue yields a transcendental equation for z that together with the assumed strain distribution constitutes the nonlinear part of the problem. The strain field is then recovered from (22), where the constant $\mathcal{A}$ is found by requiring that $w(z) = w_c$.

The problem can be solved using the approach developed in [17] with appropriate modifications accounting for the presence of second-neighbor interactions. We use a variant of the Wiener–Hopf method [31–33] and begin by extending the left hand side of the equation to the entire real axis:

$$(\alpha - 1)\int_{-z}^{z} \mathcal{Q}(x - s) h(s) ds + h(x) = \psi_-(x - z) + \psi_+(x + z), \quad -\infty < x < \infty.$$

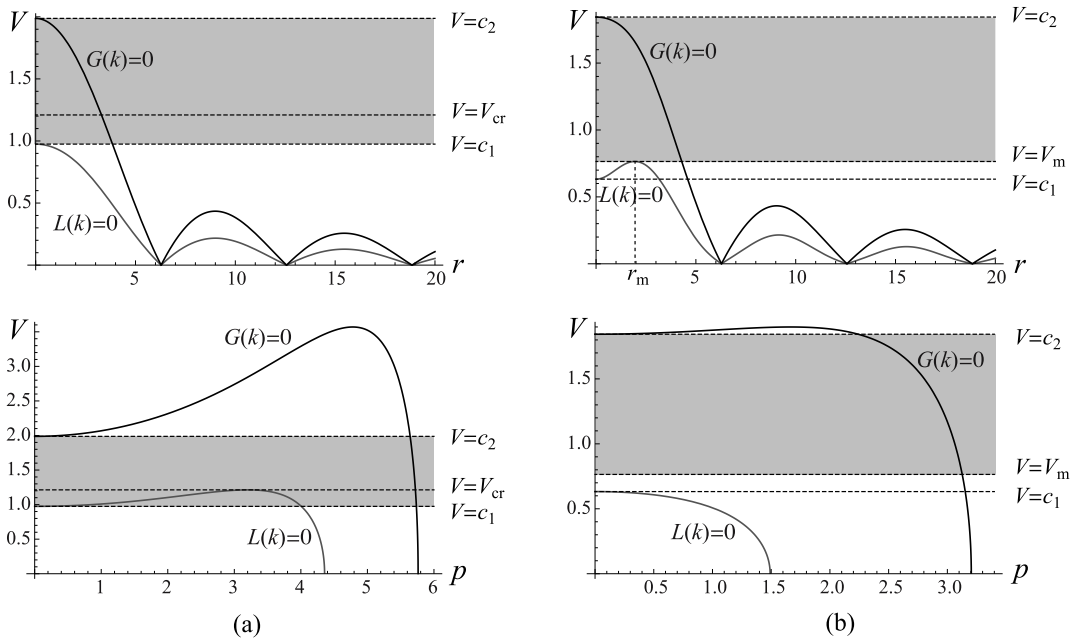

Fig. 3. Real $k = r > 0$ and imaginary $k = ip$, $p > 0$ roots of $G(k) = 0$ and $L(k) = 0$ at $\alpha = 4$ and (a) $-1/4 < \beta < 0$ ($\beta = -0.05$); (b) $-1 < \beta < -1/4$ ($\beta = -0.6$). The solitary waves involve roots inside the shaded region.

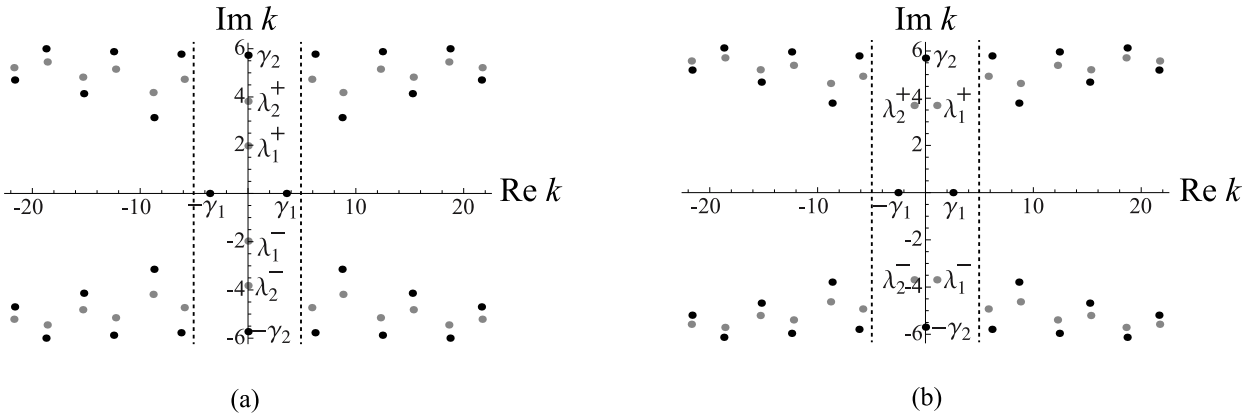

Fig. 4. Nonzero roots of $G(k) = 0$ (black circles) and $L(k) = 0$ (gray circles) at (a) $c_1 < V < V_{cr}$, $-1/4 < \beta < 0$ and (b) either $V_{cr} < V < c_2$, $-1/4 < \beta < 0$ or $V_m < V < c_2$, $-1 < \beta < -1/4$. Here the parameters are $\alpha = 4$, $\beta = -0.05$, $V = 1.1$ in (a) and $V = 1.5$ in (b). The simplest approximation with $n = 2$ includes the roots $\pm\gamma_1$, $\pm\gamma_2$ and $\lambda_1^{\pm}$, $\lambda_2^{\pm}$ located within the strip $|\mathrm{Re}k| < s_2$ marked by the dashed lines.

Here $\psi_{\pm}(x)$ are some unknown functions satisfying $\psi_-(x) \equiv 0$ for $x < 0$ and $\psi_+(x) \equiv 0$ for $x > 0$. Taking Fourier transform of both sides, we obtain

$$\frac{G(k)}{L(k)} H(k) = e^{ikz}\hat{\psi}_+(k) + e^{-ikz}\hat{\psi}_-(k), \tag{25}$$

where $\hat{\psi}_{\pm}(k)$ are Fourier transforms of $\psi_{\pm}(x)$. Using an infinite product representation [34] of the ratio $G(k)/L(k)$ in the generic case when all nonzero roots of $L(k) = 0$ and $G(k) = 0$ are simple, we have

$$\frac{c_2^2 - V^2}{c_1^2 - V^2} \frac{\prod_{i=1}^{\infty} 1 - \frac{k^2}{\gamma_i^2}}{\prod_{i=1}^{\infty}\left(1 - \frac{k}{\lambda_i^+}\right)\left(1 - \frac{k}{\lambda_i^-}\right)} H(k) = e^{ikz}\hat{\psi}_+(k) + e^{-ikz}\hat{\psi}_-(k), \tag{26}$$

where c_1 and c_2 are defined in (15) and we recall that $G(\gamma_j) = 0$ and either $\mathrm{Re}(\gamma_j) > 0$ or $\mathrm{Re}(\gamma_j) = 0$, $\mathrm{Im}(\gamma_j) > 0$, and $L(\lambda_i^+) = 0$, $\mathrm{Im}(\lambda_i^+) > 0$.

Consider now a strip $|\mathrm{Re}k| < s_n$ containing n roots γ_i and n roots λ_i^+; see Fig. 4. Due to the structure of the roots at $-1 < \beta < 0$ and V within (17), such n is necessarily even, and by symmetry the roots $-\gamma_i$ and $\lambda_i^- = \overline{\lambda_i^+}$ are also included within the strip, so that the total number of the nonzero roots of $L(k) = 0$ and $G(k) = 0$ in the nth strip is $4n$. Then (26) is approximated by

$$\frac{\prod_{i=1}^{n}(k^2 - \gamma_i^2)}{\prod_{i=1}^{n}(k - \lambda_i^+)\prod_{i=1}^{n}(k - \lambda_i^-)} H_n(k) = e^{ikz_n}\Psi_+^{(n)}(k) + e^{-ikz_n}\Psi_-^{(n)}(k), \tag{27}$$

where $H_n(k)$ and z_n approximate $H(k)$ and z, respectively, and

$$\Psi_{\pm}^{(n)}(k) = -\frac{V^2 - c_1^2}{c_2^2 - V^2}\prod_{i=1}^{n}\frac{|\gamma_i|^2}{|\lambda_i^+|^2}\hat{\psi}_{\pm}(k). \tag{28}$$

An analytic continuation argument [32,33] and some algebraic manipulations then yield

$$H_n(k) = i\sum_{j=1}^{n} \frac{\prod_{i=1}^{n}(\gamma_j - \lambda_i^-)}{\gamma_j \prod_{i=1,\, i\neq j}^{n}(\gamma_j^2 - \gamma_i^2)} \sum_{m=1}^{n} d_m^{(n)} \gamma_j^{m-1} \times e^{-i\gamma_j z_n}\left(\frac{\sin((k+\gamma_j)z_n)}{k+\gamma_j} - \frac{\sin((k-\gamma_j)z_n)}{k-\gamma_j}\right), \tag{29}$$

where the coefficients $d_m^{(n)}$ satisfy the linear system

$$\sum_{m=1}^{n}(M_n)_{jm}(z_n) d_m^{(n)} = 0, \quad j = 1, \dots, n, \tag{30}$$

with

$$(M_n)_{jm} = \gamma_j^{m-1}\left(\frac{(-1)^m e^{i\gamma_j z_n}}{\prod_{i=1}^{n}(\gamma_j - \lambda_i^-)} + \frac{e^{-i\gamma_j z_n}}{\prod_{i=1}^{n}(\gamma_j - \lambda_i^+)}\right). \tag{31}$$

We omit the details of the derivation which can be found in [17], where we considered the case $\beta = 0$.[1] The system (30) has a nontrivial solution if and only if the determinant of the $n \times n$ matrix $M_n(z_n)$ with the entries $(M_n)_{jm}(z_n)$ is zero. Therefore we obtain an algebraic equation

$$\det M_n(z_n) = 0, \tag{32}$$

allowing one to find z_n. Once z_n is found, we can solve (30) for $d_m^{(n)}$, which are determined up to an arbitrary multiplicative constant and compute $H_n(k)$, which yields [32]

$$h_n(x) = \sum_{j=1}^{n} \frac{\sin(\gamma_j x) e^{-i\gamma_j z_n} \prod_{i=1}^{n}(\gamma_j - \lambda_i^-)}{\gamma_j \prod_{i=1,\, i\neq j}^{n}(\gamma_j^2 - \gamma_i^2)} \sum_{m=1}^{n} d_m^{(n)} \gamma_j^{m-1}. \tag{33}$$

The normalization condition $\int_0^{z_n} h_n(x)dx = 1$ then selects a unique set of coefficients $d_m^{(n)}$ and yields the approximate solution $h_n(x)$ of the integral equation. The exact solution of (23) and the value of z are obtained in the limit $n \to \infty$.

Substituting into (22) the truncated approximation of $G(k)H(k)/L(k)$ that includes only the roots in the $|\mathrm{Re}k| < s_n$, recalling (27), (28), using the residue theorem as in [17] and imposing $w(\pm z_n) = w_c$, we obtain the nth approximation of the strain field:

$$w_n(x) = w_c\left(1 - \frac{V^2 - c_1^2}{d_1^{(n)}(c_2^2 - V^2)} \sum_{j=1}^{n} \frac{\prod_{i=1}^{n}\left(1 - \frac{\gamma_j}{\lambda_i^-}\right)}{\prod_{i=1,\, i\neq j}^{n}\left(1 - \frac{\gamma_j^2}{\gamma_i^2}\right)} \times e^{-i\gamma_j z_n} \sum_{m=1}^{n} d_m^{(n)} \gamma_j^{m-1}(\cos(\gamma_j x) - \cos(\gamma_j z_n))\right) \tag{34}$$

for $|x| < z_n$ and

$$w_n(x) = \frac{w_c}{d_1^{(n)}} \sum_{j=1}^{n} \frac{\sum_{m=1}^{n} d_m^{(n)}(\lambda_j^+)^{m-1}}{\prod_{i=1,\, i\neq j}^{n}\left(1 - \frac{\lambda_j^+}{\lambda_i^+}\right)} e^{i\lambda_j^+(|x| - z_n)} \tag{35}$$

for $|x| > z_n$. In particular, the amplitude of the nth approximation is given by

$$w_n(0) = w_c\left(1 - \frac{V^2 - c_1^2}{c_2^2 - V^2}\left(\prod_{i=1}^{n}|\gamma_i|\right)^2 \left(d_1^{(n)} \prod_{i=1}^{n} \lambda_i^-\right)^{-1}\right). \tag{36}$$

[1] The difference here is that n is even, while in $\beta = 0$ case it was odd [17]. This affects some symmetries taken into account in (31), where we have $(-1)^m$ in place of $(-1)^{(m-1)}$ in Eq. (9) in [17].

In the limit $n \to \infty$ (34) and (35) yield the exact solution in the form (18), with

$$a_0 = w_c\left(1 + \frac{V^2 - c_1^2}{c_2^2 - V^2} \lim_{n\to\infty} \frac{1}{d_1^{(n)}} \sum_{j=1}^{n} \frac{\prod_{i=1}^{n}\left(1 - \frac{\gamma_j}{\lambda_i^-}\right)}{\prod_{i=1,\, i\neq j}^{n}\left(1 - \frac{\gamma_j^2}{\gamma_i^2}\right)} \times e^{-i\gamma_j z_n} \sum_{m=1}^{n} d_m^{(n)} \gamma_j^{m-1} \cos(\gamma_j z_n)\right),$$

$$a_j = -w_c \frac{V^2 - c_1^2}{c_2^2 - V^2} \lim_{n\to\infty} \frac{1}{d_1^{(n)}} \frac{\prod_{i=1}^{n}\left(1 - \frac{\gamma_j}{\lambda_i^-}\right)}{\prod_{i=1,\, i\neq j}^{n}\left(1 - \frac{\gamma_j^2}{\gamma_i^2}\right)} e^{-i\gamma_j z_n} \sum_{m=1}^{n} d_m^{(n)} \gamma_j^{m-1}$$

and

$$b_j = w_c \lim_{n\to\infty} \frac{e^{-i\lambda_j^+ z_n}}{d_1^{(n)}} \frac{\sum_{m=1}^{n} d_m^{(n)}(\lambda_j^+)^{m-1}}{\prod_{i=1,\, i\neq j}^{n}\left(1 - \frac{\lambda_j^+}{\lambda_i^+}\right)}.$$

At $\beta = 0$ the sound speeds are $c_1 = 1$, $c_2 = \sqrt{\alpha}$, and we recover the solution in [17].

Note that we have assumed without proof that there exists z_n for each even n such that the corresponding $w_n(x)$ is admissible, i.e. satisfies the assumed inequalities $w_n(x) < w_c$ for $|x| > z_n$ and $w_n(x) > w_c$ for $|x| < z_n$, and that the resulting z_n, $h_n(x)$ and $w_n(x)$ sequences converge. To support these assumptions we present in the next section several explicit examples, while the general mathematical study of the ensuing problem remains to be done. We also remark that even though the nonlinear equation (32) may have more than one solution for each n, our examples show that only the smallest z_n value corresponds to an admissible field $w_n(x)$ at a given n.

An alternative procedure to obtain semianalytical solution via numerical approximation of the integral equation is described in Appendix A.

5. Approximation by low-order truncation

Here we illustrate the procedure developed in Section 4 by considering in detail the simplest approximation with $n = 2$. Some numerical evidence of convergence of the general series as $n \to \infty$ is provided in Appendix B.

The approximation $n = 2$ includes only the roots located within a strip $|\mathrm{Re}k| < s_2$, where s_2 is chosen to be large enough for the strip to contain eight roots, as shown in Fig. 4, four roots of $G(k) = 0$ and four roots of $L(k) = 0$. This means that we need to include a symmetric pair of real roots and a symmetric pair of imaginary roots of $G(k) = 0$:

$$\pm\gamma_1 = \pm r \quad \text{and} \quad \pm\gamma_2 = \pm ip, \tag{37}$$

where $r > 0$ and $p > 0$. Meanwhile, depending on V and β, the first four roots of $L(k) = 0$ are either two symmetric pairs of purely imaginary roots, corresponding to a monotone decay of solitary waves at infinity, or a complex quadruple, which yields oscillatory decay.

Solutions with a monotone decay. We begin with the first case, which occurs when $-1/4 < \beta < 0$ and $c_1 < V < V_{\mathrm{cr}}$. Recall that in this parameter regime the first four roots of $L(k) = 0$, as illustrated in Fig. 4(a), are

$$\lambda_1^+ = iq_1, \quad \lambda_2^+ = iq_2, \quad \lambda_1^- = -iq_1, \quad \lambda_2^- = -iq_2, \tag{38}$$

$$M_2(z_2) = \begin{bmatrix} \dfrac{e^{-irz_2}}{(r-iq_1)(r-iq_2)} - \dfrac{e^{irz_2}}{(r+iq_1)(r+iq_2)} & r\left(\dfrac{e^{irz_2}}{(r+iq_1)(r+iq_2)} + \dfrac{e^{-irz_2}}{(r-iq_1)(r-iq_2)}\right) \\ \dfrac{e^{-pz_2}}{(p+q_1)(p+q_2)} - \dfrac{e^{pz_2}}{(p-q_1)(p-q_2)} & (-ip)\left(\dfrac{e^{-pz_2}}{(p+q_1)(p+q_2)} + \dfrac{e^{-pz_2}}{(p-q_1)(p-q_2)}\right) \end{bmatrix}, \tag{39}$$

Box I.

where $q_2 > q_1 > 0$. In this case the 2×2 matrix M_2, defined in (31), is given by Eq. (39) in Box I where we recall that z_2 denotes the value of z in the $n = 2$ approximation in (27). Then (32) yields the nonlinear algebraic equation

$$\begin{aligned} F(z_2) &:= r[(r^2 - q_1q_2)\cos(rz_2) + r(q_1+q_2)\sin(rz_2)] \\ &\times [(p^2 + q_1q_2)\sinh(pz_2) \\ &+ p(q_1+q_2)\cosh(pz_2)] - p[(r^2 - q_1q_2)\sin(rz_2) \\ &- r(q_1+q_2)\cos(rz_2)][(p^2+q_1q_2)\cosh(pz_2) \\ &+ p(q_1+q_2)\sinh(pz_2)] = 0 \end{aligned} \tag{40}$$

In the limit $\beta \to 0$, when p and q_2 tend to infinity as $O(1/\sqrt{-\beta})$, the equation reduces to $\tan(rz_2) = -r/q_1$, which is consistent with the first-root approximation in [17]. To see that (40) has solutions $z_2 > 0$, observe that

$$\begin{aligned} F'(z_2) = &-(p^2+r^2)[(r^2 - q_1q_2)\sin(rz_2) - r(q_1+q_2)\cos(rz_2)] \\ &\times [(p^2+q_1q_2)\sinh(pz_2) + p(q_1+q_2)\cosh(pz_2)]. \end{aligned}$$

Under our assumptions, $F'(z_2)$ vanishes at infinitely many values $z_2^* > 0$ satisfying

$$(r^2 - q_1q_2)\sin(rz_2^*) - r(q_1+q_2)\cos(rz_2^*) = 0$$

and corresponding to the maxima and minima of $F(z_2)$, where we have

$$\begin{aligned} F(z_2^*) = &\frac{(q_1^2+r^2)(q_2^2+r^2)}{q_1+q_2}\sin(rz_2^*)[(p^2+q_1q_2)\sinh(pz_2^*) \\ &+p(q_1+q_2)\cosh(pz_2^*)]. \end{aligned}$$

Clearly, $F(z_2^*)$ changes sign as $\sin(rz_2^*)$ changes sign, which implies that $F(z_2) = 0$ has infinitely many positive solutions. One can show that only the first positive solution of (47) corresponds to an admissible solitary wave profile that satisfies the assumed strain distribution, so in what follows only this value of z_2 is considered.

Note that $F(0) = pr(q_1+q_2)(p^2+r^2) > 0$, so in the limit $V \to c_1$, the lower velocity limit at $-1/4 < \beta < 0$, we have $q_1 \approx \sqrt{\frac{12(V^2-c_1^2)}{1+4\beta}} \to 0$, while q_2, p and r tend to finite positive limits, we have $F(0)$ approaching a positive value. This implies that z_2 is strictly positive in the limit $V \to c_1$.

The shape function (33) in this case reduces to

$$\begin{aligned} h_2(x) = &\frac{(r+iq_1)(r+iq_2)}{r(r^2+p^2)}e^{-irz_2}(d_1^{(2)} + d_2^{(2)}r)\sin(rx) \\ &+\frac{(p+q_1)(p+q_2)}{p(p^2+r^2)}e^{pz_2}(d_1^{(2)} + id_2^{(2)}p)\sinh(px), \end{aligned}$$

where the roots are given by (37), (38), and the constants $d_1^{(2)}$, $d_2^{(2)}$ are obtained from the first equation of the singular system (30) with $n = 2$ after some algebraic manipulations and the constraint $\int_0^{z_2} h_2(x)dx = 1$. They are given by

$$\begin{aligned} d_1^{(2)} &= r(p^2+r^2)((r^2 - q_1q_2)\cos(rz_2) \\ &\quad + r(q_1+q_2)\sin(rz_2))/\Delta(z_2), \\ d_2^{(2)} &= -i(p^2+r^2)(r(q_1+q_2)\cos(rz_2) \\ &\quad + (q_1q_2 - r^2)\sin(rz_2))/\Delta(z_2), \end{aligned} \tag{41}$$

where

$$\begin{aligned} \Delta(z_2) = &\frac{1}{2p^2r}\Big[2p^2(q_1^2+r^2)(q_2^2+r^2) + (e^{pz_2}-1)^2(p+q_1) \\ &\times (p+q_2)r[pq_1q_2 + (q_1+q_2-p)r^2]\sin(rz_2) \\ &+ \cos(rz_2)\{(e^{pz_2}-1)^2p^3(q_1+q_2)r^2 + (e^{pz_2}-1)^2p(q_1+q_2)r^4 \\ &- (e^{pz_2}-1)^2q_1q_2r^2(q_1q_2 - r^2) \\ &+ p^2[(e^{pz_2}-1)^2q_1q_2r^2 - q_1^2(2q_2^2 - 2e^{pz_2}r^2(\sinh(pz_2)-1)) \\ &+ 2e^{pz_2}r^2(q_2^2+r^2)(\sinh(pz_2)-1)]\}\Big]. \end{aligned}$$

The strain $w_2(x)$ is obtained from (34), (35) with the roots given by (37), (38):

$$\begin{aligned} w_2(x) = &w_c\Bigg(1 - \frac{V^2 - c_1^2}{d_1^{(2)}(c_2^2 - V^2)q_1q_2(p^2+r^2)} \\ &\times \Big[p^2(q_1 - ir)(q_2 - ir)e^{-irz_2}(d_1^{(2)} + d_2^{(2)}r)(\cos(rx) \\ &- \cos(rz_2)) + r^2(p+q_1)(p+q_2)e^{pz_2}(d_1^{(2)} + id_2^{(2)}p) \\ &\times (\cosh(px) - \cosh(pz_2))\Big]\Bigg), \quad |x| < z_2, \end{aligned} \tag{42}$$

$$\begin{aligned} w_2(x) = &\frac{w_c}{d_1^{(2)}(q_2 - q_1)}\Big[q_2(d_1^{(2)} + id_2^{(2)}q_1)e^{-q_1(|x|-z_2)} \\ &-q_1(d_1^{(2)} + id_2^{(2)}q_2)e^{-q_2(|x|-z_2)}\Big], \quad |x| > z_2, \end{aligned} \tag{43}$$

where the coefficients $d_1^{(2)}$ and $d_2^{(2)}$ are given by (41). The top left panel ($V = 0.8989$) in Fig. 5 shows a typical solution profile in this regime together with the semi-analytical solution obtained using the trapezoidal approximation, as described in Appendix A. One can see that the first-roots approximation captures the monotonely decaying solution very well.

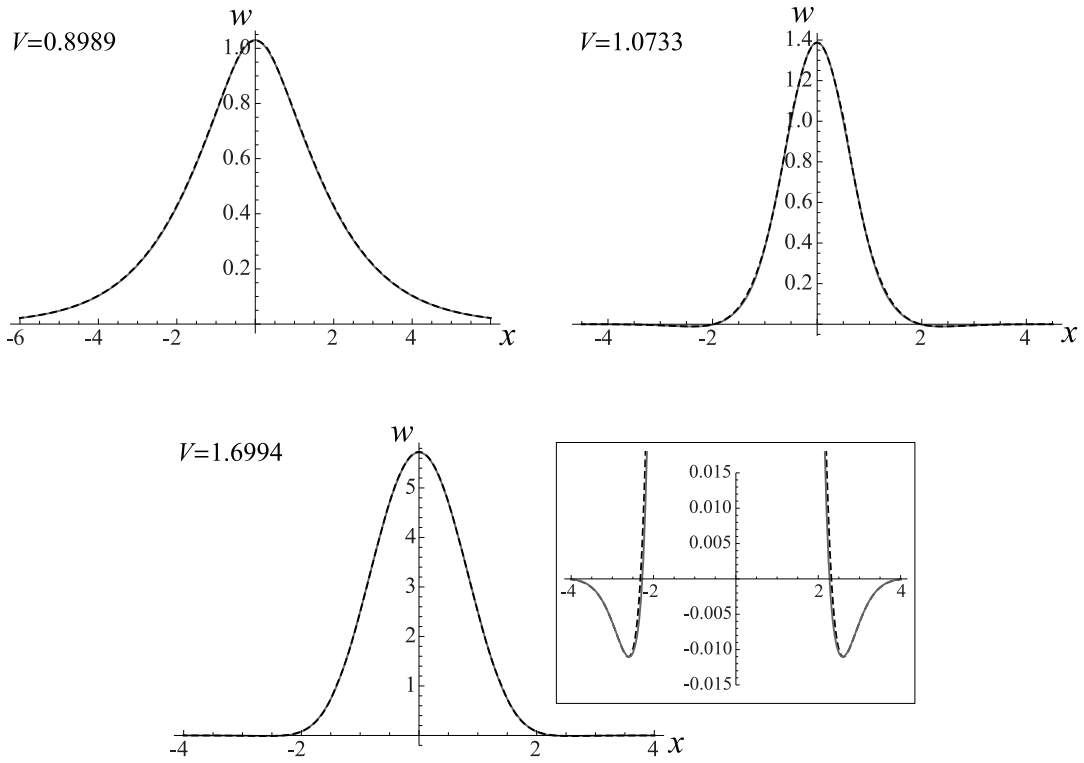

Fig. 5. Strain profiles obtained from the semi-analytical solution (solid gray curves) and the $n = 2$ approximation (dashed black curves). Here $\alpha = 4$, $\beta = -0.2$, which yield $c_1 \approx 0.8944$, $V_{\rm cr} \approx 0.9$ and $c_2 \approx 1.9494$, and $w_c = 1$. The top left panel corresponds to the case $c_1 < V < V_{\rm cr}$ (monotone decay), while in the other two panels $V_{\rm cr} < V < c_2$ (oscillatory decay).

The amplitude of the solitary wave is given by

$$w_2(0) = w_c\left(1 + \frac{(V^2 - c_1^2)p^2r^2}{(c_2^2 - V^2)d_1^{(2)}q_1q_2}\right), \quad c_1 < V < V_{\rm cr}, \\ -1/4 < \beta < 0, \tag{44}$$

where we used (36) with $n = 2$. Consider now the lower velocity limit $V \to c_1$ and recall that in this limit $q_1 \approx \sqrt{\frac{12(V^2-c_1^2)}{1+4\beta}} \to 0$, while q_2, p, r and, as can be shown, $d_1^{(2)}$ tend to finite positive values. This implies that $w_2(0) \to w_c$, and the solution approaches $w(x) = w_c$ for all x. In other words, in this limit the solution delocalizes into a straight line at the critical strain, as in the sonic limit in the $\beta = 0$ case [17].

Solutions with an oscillatory decay. We now consider the case when either $-1 < \beta < -1/4$ and $V_{\rm m} < V < c_2$ or $-1/4 < \beta < 0$ and $V_{\rm cr} < V < c_2$. Then, as illustrated in Fig. 4(b), the roots are

$$\lambda_1^+ = \xi + i\eta, \quad \lambda_2^+ = -\xi + i\eta, \quad \lambda_1^- = \xi - i\eta, \\ \lambda_2^- = -\xi - i\eta, \tag{45}$$

where $\xi > 0$ and $\eta > 0$. In this case M_2 is given by Eq. (46) in Box II. Eq. (32) then yields the following nonlinear equation for z_2:

$$F(z_2) := r[(r^2 - \eta^2 - \xi^2)\cos(rz_2) + 2r\eta\sin(rz_2)] \\ \times [(\xi^2 + p^2 + \eta^2)\sinh(pz_2) + 2p\eta\cosh(pz_2)] \\ - p[(r^2 - \eta^2 - \xi^2)\sin(rz_2) - 2r\eta\cos(rz_2)] \\ \times [(\xi^2 + p^2 + \eta^2)\cosh(pz_2) + 2p\eta\sinh(pz_2)] = 0. \tag{47}$$

As in the previous case, we can show that (47) has infinitely many positive solutions, of which we again select the relevant first root.

Observe that $F(0) = 2pr\eta(r^2 + p^2) > 0$ and that $F(0) \to 0$ as $\eta \to 0$ when V approaches the lower velocity limit $V_{\rm m}$ at $< -1 < \beta < -1/4$, so in the limit $V \to V_{\rm m}$ we have $z_2 \to 0$. As the velocity increases, p and r monotonically decrease, while η and ξ monotonically increase, so that z_2 grows. At large pz_2, $\cosh(pz_2) \approx \sinh(pz_2)$, so z_2 is well approximated by

$$z_2 \approx \frac{1}{r}\left(\pi - \arctan\frac{r(r^2 - \eta^2 - \xi^2 + 2p\eta)}{p(\eta^2 + \xi^2 - r^2) + 2r^2\eta}\right). \tag{48}$$

Suppose $\alpha > -4\beta$ (note that this inequality always holds if $-1/4 < \beta < 0$, since then $\alpha > 1 > -4\beta$, but may fail if $-1 < \beta < -1/4$). Then as $V \to c_2$, we have $r \to 0$, while the other roots have finite nonzero limits, so we have $z_2 \approx \pi/r \to \infty$ in the upper sonic limit. If $-1 < \beta < -1/4$ and $1 < \alpha < -4\beta$, we have $p \to 0$ as $V \to c_2$, while the other roots tend to finite nonzero limits, so in this case z_2 approaches a finite nonzero value solving the transcendental equation

$$r(2\eta + (\eta^2 + \xi^2)z)\left(2\eta r\sin(rz) - (\eta^2 - r^2 + \xi^2)\cos(rz)\right) \\ + (\eta^2 + \xi^2)\left(2\eta r\cos(rz) + (\eta^2 - r^2 + \xi^2)\sin(rz)\right) = 0,$$

obtained by expanding (47) at small p.

Using (33), (37) and (45), we obtain the shape function

$$h_2(x) = \frac{(r + i\eta)^2 - \xi^2}{r(r^2 + p^2)}e^{-irz_2}(d_1^{(2)} + d_2^{(2)}r)\sin(rx) \\ + \frac{(p + \eta)^2 + \xi^2}{p(p^2 + r^2)}e^{pz_2}(d_1^{(2)} + id_2^{(2)}p)\sinh(px),$$

$$M_2(z_2)=\begin{bmatrix} \dfrac{e^{-irz_2}}{(r-i\eta)^2-\xi^2}-\dfrac{e^{irz_2}}{(r+i\eta)^2-\xi^2} & r\left(\dfrac{e^{irz_2}}{(r+i\eta)^2-\xi^2}+\dfrac{e^{-irz_2}}{(r-i\eta)^2-\xi^2}\right) \\ \dfrac{e^{-pz_2}}{(p+\eta)^2+\xi^2}-\dfrac{e^{pz_2}}{(p-\eta)^2+\xi^2} & (-ip)\left(\dfrac{e^{-pz_2}}{(p+\eta)^2+\xi^2}+\dfrac{e^{pz_2}}{(p-\eta)^2+\xi^2}\right) \end{bmatrix}. \tag{46}$$

Box II.

where the constants $d_1^{(2)}$, $d_2^{(2)}$ are obtained as before from the first equation of (30) and the constraint on $h_2(x)$ and are given by

$$\begin{aligned} d_1^{(2)} &= r(p^2+r^2)((r^2-\xi^2-\eta^2)\cos(rz_2) \\ &\quad +2r\eta\sin(rz_2))/\Delta(z_2), \\ d_2^{(2)} &= -i(p^2+r^2)(2r\eta\cos(rz_2) \\ &\quad -(r^2-\xi^2-\eta^2)\sin(rz_2))/\Delta(z_2), \end{aligned} \tag{49}$$

where

$$\begin{aligned} \Delta(z_2) &= -(r^4+2r^2(\eta^2-\xi^2)+(\xi^2+\eta^2)^2)(\cos(rz_2)-1)/r \\ &+ (1/p^2)e^{pz_2}(\xi^2+(p+\eta)^2)(\cosh(pz_2)-1) \\ &\times [r(r^2-\xi^2+2p\eta-\eta^2)\cos(rz_2) \\ &+ (2r^2\eta+p(\xi^2+\eta^2-r^2))\sin(rz_2)]. \end{aligned} \tag{50}$$

Recovering the strain field from (34), (35) with the roots given by (37), (45), we obtain

$$\begin{aligned} w_2(x) =& w_c\Bigg(1-\frac{V^2-c_1^2}{d_1^{(2)}(c_2^2-V^2)(p^2+r^2)(\xi^2+\eta^2)} \\ &\times\Big[p^2(\xi^2+(\eta-ir)^2)e^{-irz_2}(d_1^{(2)}+d_2^{(2)}r)(\cos(rx) \\ &-\cos(rz_2))+r^2(\xi^2+(\eta+p)^2)e^{pz_2}(d_1^{(2)}+id_2^{(2)}p) \\ &\times(\cosh(px)-\cosh(pz_2))\Big]\Bigg), \quad |x|<z_2, \\ w_2(x) =& \frac{w_c}{2d_1^{(2)}\xi}\Big[(\xi-i\eta)(d_1^{(2)}+d_2^{(2)}(\xi+i\eta))e^{(-\eta+i\xi)(|x|-z_2)} \\ &+(\xi+i\eta)(d_1^{(2)}+d_2^{(2)}(-\xi+i\eta))e^{(-\eta-i\xi)(|x|-z_2)}\Big], \\ &|x|>z_2, \end{aligned} \tag{51, 52}$$

where the coefficients $d_1^{(2)}$ and $d_2^{(2)}$ are given by (49).

Typical solution profiles are shown in the top right and bottom panels of Fig. 5 ($V=1.0733$ and $V=1.6994$) for $-1/4<\beta<0$ and $V_{cr}<V<c_2$ and in Fig. 6 for $-1<\beta<-1/4$ and $V_m<V<c_2$. One can see an excellent agreement between the $n=2$ approximation (dashed black curves) and the semi-analytical solution (solid gray curves). As expected, solutions exhibit decaying oscillations in all cases except when $-1/4<\beta<0$ and $c_1<V<V_{cr}$ (the top left panel in Fig. 5, $V=0.8989$). At $-1<\beta<-1/4$ the oscillations are more pronounced than in the smaller-$|\beta|$ case, and their amplitude increases as the lower velocity limit V_m is approached.

From (36) we find that the amplitude of the solitary wave is given by

$$w_2(0)=w_c\left(1+\frac{(V^2-c_1^2)p^2r^2}{(c_2^2-V^2)d_1^{(2)}(\xi^2+\eta^2)}\right), \tag{53}$$

$$\begin{cases} V_{cr}<V<c_2, & -1/4<\beta<0 \\ V_m<V<c_2, & -1<\beta<-1/4 \end{cases}$$

In the limit $V\to V_m$ at $-1<\beta<-1/4$, when $\eta\to 0$ and $z_2\to 0$, as discussed above, we have $\Delta(z_2)\to 0$ in (50) and therefore $d_1^{(2)}\to\infty$ in (49), so the amplitude tends to w_c in this limit, while the solution approaches a non-decaying linear wave $w(x)=w_c\cos(k_m x)$ (dashed curve in Fig. 7(b)), where we recall that k_m is the limit of ξ when $V\to V_m$. At velocities just above V_m the solution $w(x)$ has the envelope-soliton form, as illustrated by the solid curve in Fig. 7.

Solution behavior in the upper velocity limit, $V\to c_2$, depends on the sign of $\alpha+4\beta$. Consider first the case when $\alpha>-4\beta$ for any β in $(-1,0)$ (with $\alpha>1$). As discussed above, in this case $r\to 0$ and $z_2\to\infty$, and one can show that $d_1^{(2)}\approx p^2r^2/(2(\eta^2+\xi^2))$ near the upper sonic limit. As a result, the asymptotic behavior of the amplitude (53) is

$$w_2(0)\approx\frac{2(\alpha-1)}{c_2^2-V^2}w_c, \quad V\to c_2, \tag{54}$$

and it becomes infinite in the limit. Turning now to the case when $-1<\beta<-1/4$ and $1<\alpha<-4\beta$, recall that in this parameter regime $p\to 0$ as $V\to c_2$, while the other roots and z_2 remain nonzero and finite in the limit. One can show that this yields a finite positive limit for $d_1^{(2)}$. Since $p^2\approx 12(V^2-c_2^2)/(\alpha+4\beta)$ for velocities just below c_2, the limit of the amplitude (53) is also finite in this case:

$$w_2(0)\to w_c\left(1-\frac{12(\alpha-1)r^2}{(\alpha+4\beta)d_1^{(2)}(\xi^2+\eta^2)}\right), \quad V\to c_2, \tag{55}$$

where r, ξ, η and $d_1^{(2)}$ denote the limiting values of the corresponding quantities.

6. Numerical analysis of stability

To study stability of the obtained traveling wave solutions one needs to consider the initial value problem for the original system (3) of ordinary differential equations. In this section we present the results of numerical simulations for the chain with M mass points, where M is chosen to be large enough to avoid reflections of waves from the boundaries during the time of the computation. We use the standard fourth-order Runge–Kutta method with small enough fixed time step ($\Delta t=0.001$) to ensure approximate energy conservation and boundary conditions $w_0=w_1=w_M=w_{M+1}=0$. Two types of initial data are considered.

The first type of initial conditions are constructed from the semi-analytical solitary wave solution at a given V (computed numerically using the trapezoidal approximation as described in

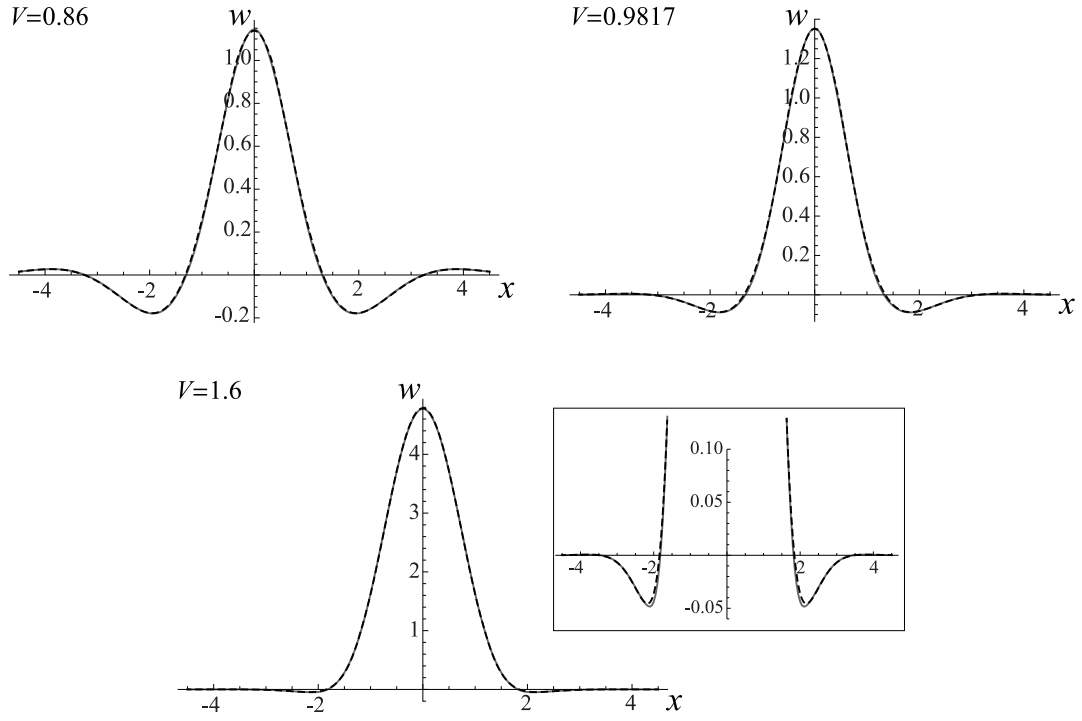

Fig. 6. Strain profiles obtained from the semi-analytical solution (solid gray curves) and the $n = 2$ approximation (dashed black curves). Here $\alpha = 4$, $\beta = -0.4$, which yield $V_{\rm m} \approx 0.8057$ (the lower velocity limit) and $c_2 \approx 1.8974$, and $w_c = 1$.

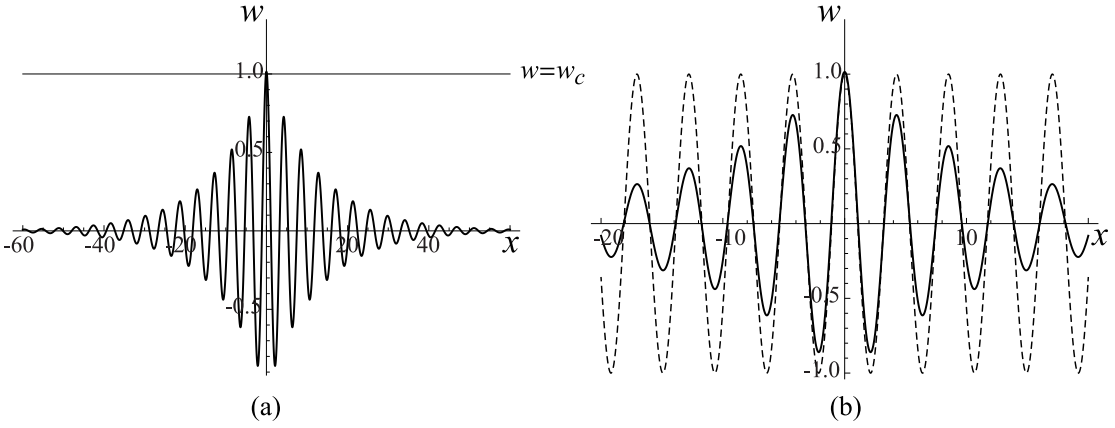

Fig. 7. (a) Solitary wave solution at $V = 0.806 > V_{\rm m}$ at $\alpha = 4$ and $\beta = -0.4$, which yield $V_{\rm m} \approx 0.8057$. Its amplitude is slightly above $w_c = 1$. (b) The same solution (solid curve) is shown over a smaller x-interval together with the linear wave $\cos(k_{\rm m}x)$ (dashed curve) approached in the limit $V \to V_{\rm m}$.

Appendix A), which is truncated and padded by zeros to create a small perturbation:

$$
\begin{aligned}
&w_n(0) = w(n - n_0), \quad \dot w_n(0) = -V w'(n - n_0),\\
&|n - n_0| \le n_{\rm tr},\\
&w_n(0) = \dot w_n(0) = 0,\\
&\quad 1 \le n < n_0 - n_{\rm tr} \quad \text{or} \quad n_0 + n_{\rm tr} < n \le M,
\end{aligned}
\tag{56}
$$

where we typically set $n_0 = 100$, $n_{\rm tr} = 45$, $M = 400$. We fix $\alpha = 4$, $w_c = 1$ in all simulations and consider two different values of β, $\beta = -0.2$ and $\beta = -0.4$ that are above and below, respectively, the threshold value -0.25. Recall that solitary waves exist in the velocity intervals (17), which translate into $0.8944 < V < 1.9494$ for $\beta = -0.2$ and $0.8057 < V < 1.7974$ for $\beta = -0.4$. Note that in the latter case $-1 < \beta < -1/4$, and thus, as discussed above, the lower limit $V_{\rm m} = 0.8057$ is above the sound speed $c_1 = 0.7746$. Running simulations with initial conditions (56) constructed from solitary waves with different velocities in the corresponding intervals, we find that there is a threshold velocity value V_* below which the solitary waves appear to be unstable since the initial solitary wave is eventually destroyed, and a wave in the first linear regime ($w < w_c$) develops instead after a large enough time, which increases as the threshold value is approached. This instability is illustrated in Fig. 8, where the threshold values are $V_* \approx 0.93$ at $\beta = -0.2$ (panel a) and $V_* \approx 0.84$ at $\beta = -0.4$ (panel b).

Using initial conditions with velocities above the threshold value we observe steady propagation of solitary waves with velocity, amplitude, half-width z of the core region and profile very close to the ones for the initial wave, suggesting that the corresponding solitary waves are stable. These values are computed from the numerical data (interpolated in time) as follows. To calculate the velocity $V_{\rm num}$ of the solitary wave in the numerical solution, we recall that the traveling wave ansatz implies that $w_{n+1}(t + 1/V) =$

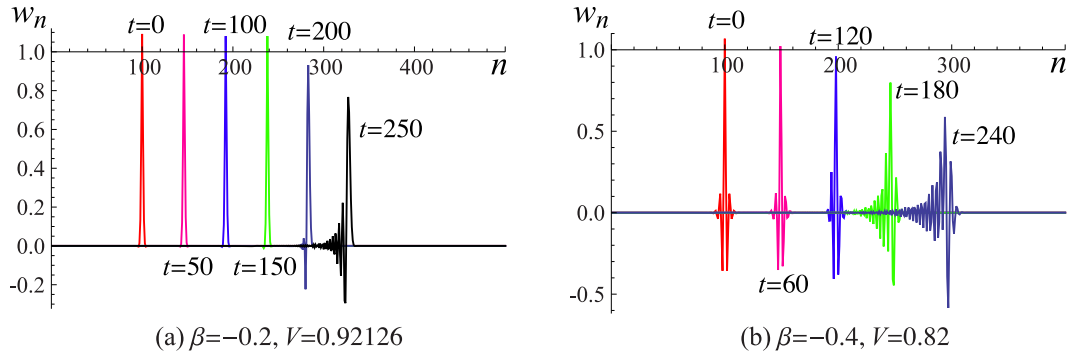

Fig. 8. Time snapshots of the numerical solutions with initial conditions (56) formed from solitary waves with velocities below the corresponding threshold values, $V_* \approx 0.93$ in (a) and $V_* \approx 0.84$ in (b). Here $\alpha = 4$ and $w_c = 1$.

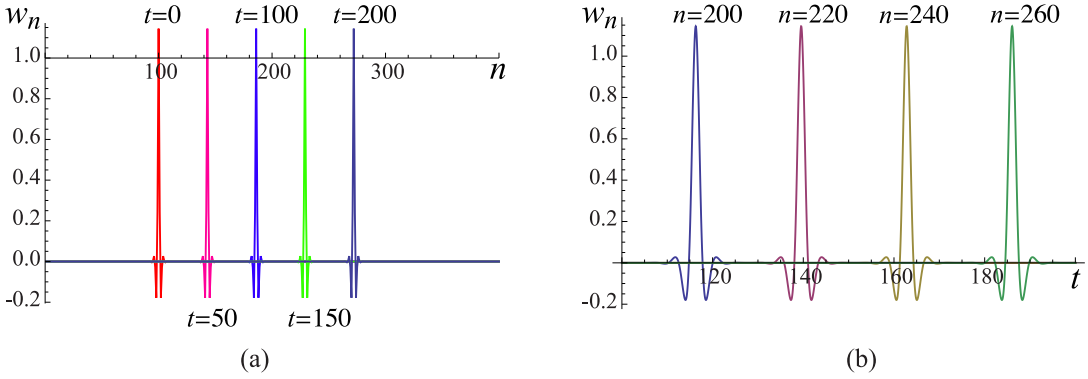

Fig. 9. (a) Time snapshots and (b) tile evolution of the numerical solutions with initial conditions (56) formed from the solitary wave with $V = 0.86$, above the threshold value $V_* \approx 0.84$. Here $\alpha = 4$, $\beta = -0.4$ and $w_c = 1$.

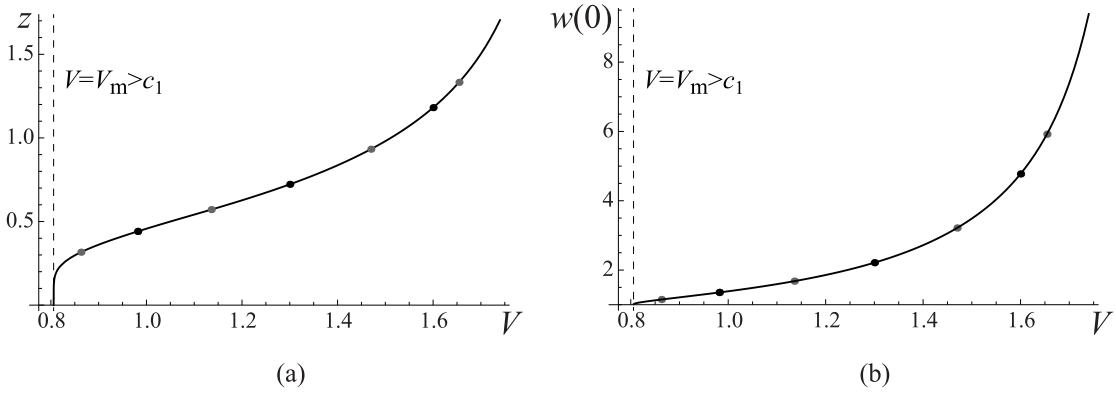

Fig. 10. Comparison of (a) the relation $z(V)$ and (b) the corresponding amplitude–velocity relation at $\alpha = 4$, $\beta = -0.4$ and $w_c = 1$ obtained from the semi-analytical solution (solid curves) and the results of the numerical simulations (circles) above the threshold velocity. Black circles indicate the results of numerical simulations with initial conditions (56), gray circles are the results of simulations with initial data (57).

$w_n(t)$, which yields $V_{\text{num}} = 1/(t_2 - t_1)$, where t_1 and t_2 are the first time instances when $w_n(t_1) = w_{n+1}(t_2) = w_c$ and n is chosen large enough so that t_1 and t_2 are near the end of the computation. The amplitude of the solitary wave in the numerical simulation is then found from $A_{\text{num}} = w_n((t_1 + T_1)/2)$, where $T_1 > t_1$ is the second time instant when $w_n(T_1) = w_c$, and the half-width of the core region is determined from $z_{\text{num}} = (T_1 - t_1)V_{\text{num}}/2$. An example of an apparently stable solitary is presented in Fig. 9, which shows time snapshots of the solutions (panel a) and time evolution $w_n(t)$ at different n (panel b) for simulations initialized by a solitary wave with $V = 0.86$ at $\beta = -0.4$. The numerical solution yields a solitary wave with slightly lower velocity, amplitude and z value (with differences of $O(10^{-5})$). This excellent agreement persists throughout the entire range $V_* < V < c_2$, as one can see in Figs. 10 and 11, which compare $z(V)$ and amplitude–velocity data obtained from numerical simulations (black circles) with the semi-analytical results.

To probe robustness of the solitary waves in a larger domain, we now consider a more generic type of initial conditions with exponentially localized initial profile

$$w_n(0) = A_0 \exp\left(-\frac{1}{2}\left|n - \frac{M}{2}\right|^2\right), \quad \dot{w}_n(0) = 0, \tag{57}$$

where the amplitude A_0 served as a parameter. At sufficiently small amplitudes, e.g. $A_0 < 1.763$ at $\beta = -0.2$, the long-time behavior corresponds again to a solution of the linear equation with $w < w_c$. For larger A_0 the initial data evolved into two solitary waves propagating towards different ends of the chain and separating

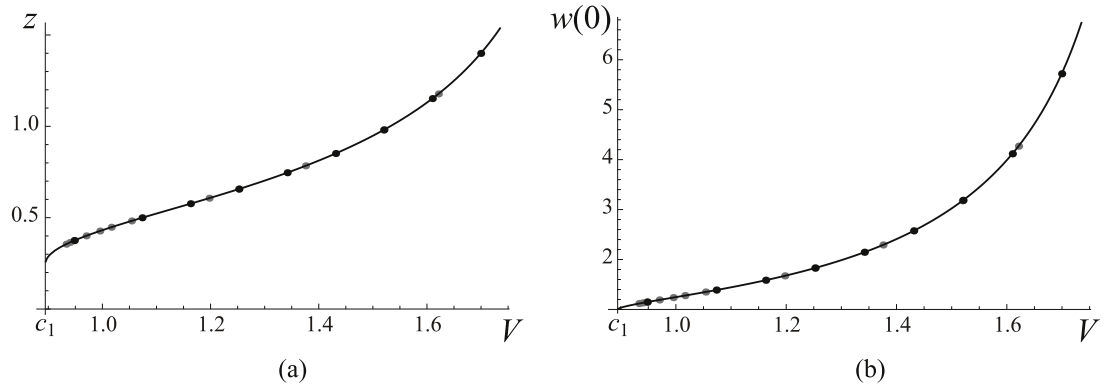

Fig. 11. Comparison of (a) the relation $z(V)$ and (b) the corresponding amplitude–velocity relation at $\alpha = 4$, $\beta = -0.2$ and $w_c = 1$ obtained from the semi-analytical solution (solid curves) and the results of the numerical simulations (circles) above the threshold velocity. Black circles indicate the results of numerical simulations with initial conditions (56), gray circles are the results of simulations with initial data (57).

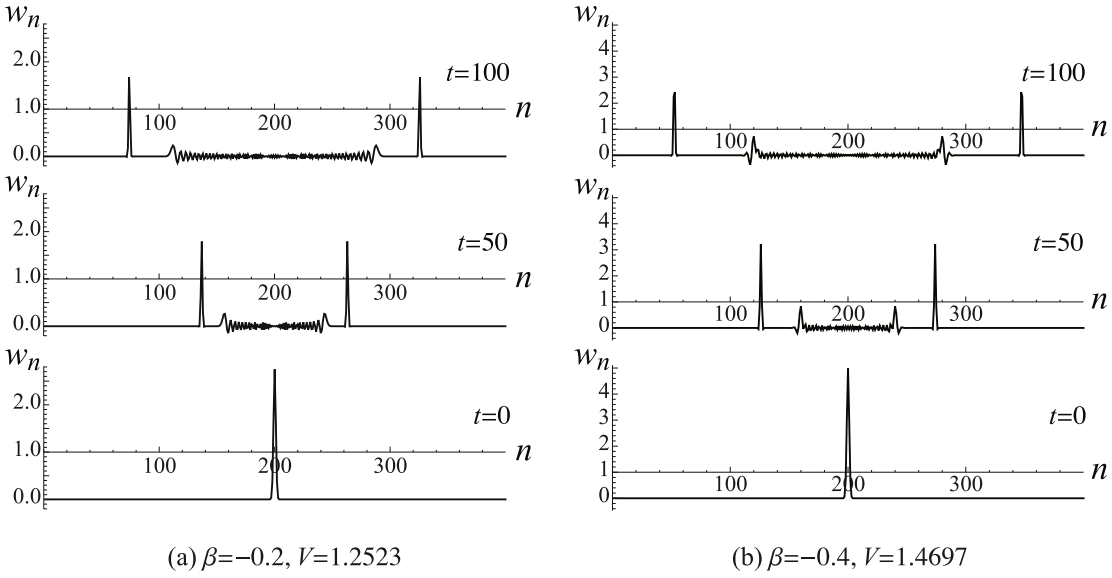

Fig. 12. Time snapshots of the numerical solutions with initial conditions (57) with $A_0 = 2.75$, $\beta = -0.2$ in panel (a) and $A_0 = 5$, $\beta = -0.4$ in panel (b). In both cases the numerical simulations yield two symmetric solitary waves propagating in opposite directions with indicated velocities. Here $\alpha = 4$ and $w_c = 1$.

from the linear waves formed in the middle of the chain; see Fig. 12 for examples. The threshold initial amplitude value of A_0 corresponds to the threshold velocity V_*. A broad agreement with semi-analytical results is again seen for $V > V_*$ in Figs. 10 and 11, where results of the numerical simulations with initial conditions (57) are marked by gray circles. The results again suggest stability of solitary waves with $V_* < V < c_2$.

To understand why stability apparently changes at V_*, we compute the energy (1) of the chain as a function of V using (A.5) and (A.7). The results are shown in Fig. 13. One can see that the energy of the solitary wave tends to infinity in the lower velocity limit, $V \to c_1$ at $1/4 < \beta \leq 0$ and $V \to V_m$ at $-1 < \beta < -1/4$, since in the former case $w(x) \to w_c$, while in the latter case the solution approaches a non-decaying linear wave in the limit. The energy also diverges in the upper limit $V \to c_2$ because the amplitude of the solitary wave goes to infinity. As velocity parameter V varies from the lower to upper limits, the energy $\mathcal{H}(V)$ first decreases, reaching a minimum value at some value and then monotonically increases. In the present examples, the velocity where $\mathcal{H}$ is minimal is around $V = V_*$ and thus coincides with the stability threshold in the simulations. Following [35,17], we conjecture that $d\mathcal{H}/dV > 0$ is at least a necessary condition for stability, so that $d\mathcal{H}/dV < 0$ indicates unstable solutions. This is analogous to the Vakhitov–Kolokolov criterion [36] widely used for the study of soliton stability in continuous systems including the nonlinear Schrödinger equation. The conjecture is consistent with the result recently proved in [37,38] for smooth potentials that the critical velocity V_* such that $\mathcal{H}'(V_*) = 0$ constitutes a threshold for instability of traveling waves in a Hamiltonian lattice.

7. Quasicontinuum approximations

Having analyzed the main features of solitary wave solutions of the discrete model, we now investigate whether they can be adequately captured by a quasicontinuum approximation. In what follows, we consider the entire parameter range $\beta > -1$ and deal with general nonlinear interaction forces $f(w)$ satisfying the conditions stated in Section 2.

7.1. Low-order approximations

We begin with the two commonly used low-order quasicontinuum approximations and explain why they fail to reproduce some

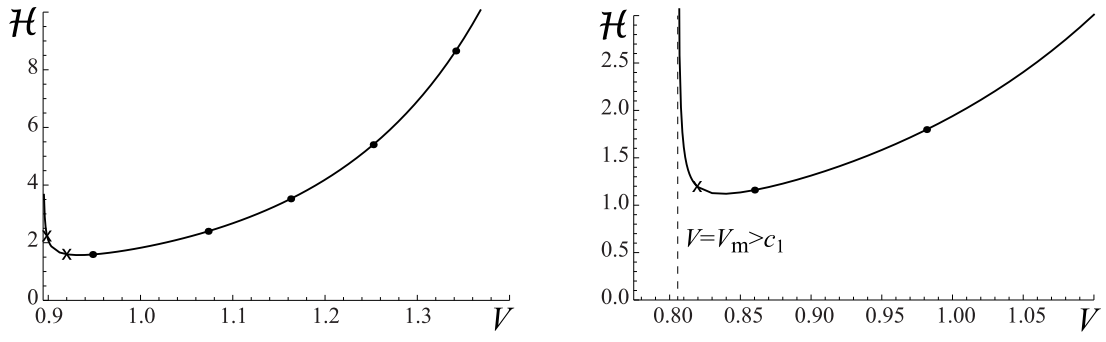

Fig. 13. The Hamiltonian (energy) of the system as a function of V at (a) $\beta = -0.2$; (b) $\beta = -0.4$. In both cases $\alpha = 4$ and $w_c = 1$. Black circles and crosses mark velocities at which the solitary wave solutions were found stable and unstable, respectively, in the numerical simulations.

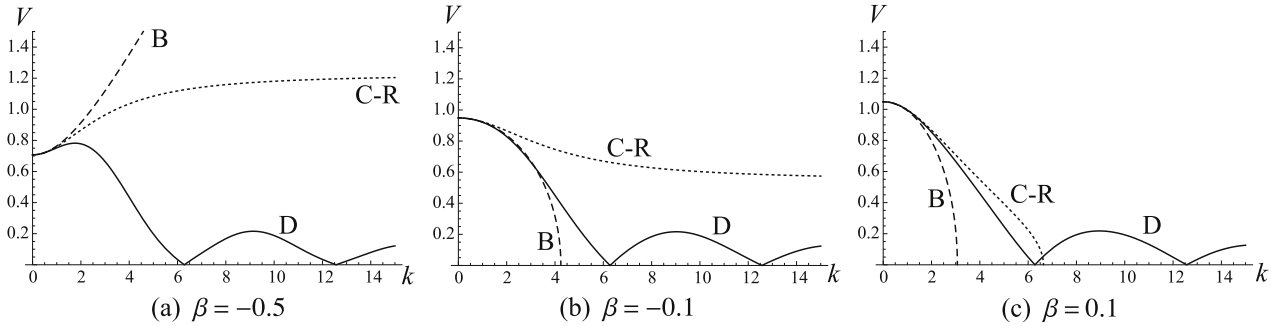

Fig. 14. Real roots of the zero-strain characteristic equations for the Boussinesq model (59) (dashed curves, B), Collins–Rosenau model (64) (dotted curves, C–R) and the discrete model (solid curves, D) at (a) $\beta = -0.5$, (b) $\beta = -0.1$ and (c) $\beta = 0.1$.

important features of the discrete model when the interactions are competitive.

Consider first the Boussinesq-type quasicontinuum approximation [39,8]. Let $u(y, t)$ be a slowly varying approximation of the small displacement $u_n(t)$, where y is a spatial variable. Expanding (2) in Taylor series and keeping second-order derivatives of all terms but fourth-order derivatives of only linear terms we obtain

$$u_{tt} = (f(u_y) + \beta u_y)_y + \frac{1+4\beta}{12} u_{yyyy}. \tag{58}$$

The fourth-order spatial derivative corresponds to a quadratic strain-gradient term in the energy [39]. Seeking traveling wave solution in the form $u(y, t) = \hat{u}(x)$, $x = y - Vt$, with $w(x) = \hat{u}'(x)$, integrating and taking into account the fact that strain $w(x)$ vanishes at infinity, we arrive at the following second-order nonlinear ordinary differential equation for $w(x)$:

$$\frac{1+4\beta}{12} w'' + (\beta - V^2)w + f(w) = 0. \tag{59}$$

Linearization of (59) about $w = 0$ yields the characteristic equation

$$V^2 = c^2 - \frac{1+4\beta}{12} k^2, \tag{60}$$

where k is the wave number associated with the plane wave solution $w = e^{ikx}$ of the linearized problem, and c defined in (9) is the corresponding sound speed. For each $V > 0$ this equation yields a symmetric pair of either real or purely imaginary roots, depending on the signs of $V - c$ and $1 + 4\beta$. Fig. 14 compares the corresponding real roots (dashed curves) to the ones for the discrete model at different values of β.

Note that for $\beta > -1/4$ the Boussinesq model correctly predicts existence of real roots at subsonic velocities, and hence requires solitary waves to be supersonic; see, e.g. Fig. 14(b,c). In the supersonic regime the two symmetric roots are purely imaginary, so the decay to zero is always monotone. However, at $-1 < \beta < -1/4$ the second-order characteristic equation (60) only captures the convexity of the discrete $V(k)$ curve at $k = 0$ and not the subsequent peak, as can be seen in Fig. 14(a). Thus, in this case the quasicontinuum approximation yields real roots for all supersonic velocities and no such roots in the subsonic regime (where the roots are purely imaginary). Hence it predicts *subsonic* solitary waves in this parameter range, in contrast to the discrete model, which, as we saw, *excludes* this possibility due to the existence of nonzero real roots at $V \le c$. The Boussinesq model does not allow any supersonic waves in this regime, while the discrete model allows strictly supersonic ones. These results are illustrated in Fig. 15(a), which should be compared to the diagram in Fig. 2(b) for the discrete model. As pointed out in [8], supersonic waves at $\beta > -1/4$ can only exist for strains on the superlinear side of the interaction force $f(w)$, while subsonic waves allowed by this model for $-1 < \beta < -1/4$ require strains to be on the sublinear side. For example, for quadratic interaction force $f(w) = w + aw^2$, the model yields supersonic solitary waves when $\beta > -1/4$ and $a > 0$ and subsonic waves when $-1 < \beta < -1/4$ and $a < 0$. Note also that since the characteristic equation (60) for the quasicontinuum model has only purely imaginary roots in the parameter regions where solitary waves may exist, the decay at infinity is always monotone, while the discrete model also allows oscillatory decay.

An advantage of a simple model like (59) is that it can be solved by quadrature, which yields explicit solutions for commonly used interaction potentials, such as cubic and quartic ones [8]. Indeed, one can integrate (59) and use the fact that strain vanishes at infinity to obtain

$$\frac{1+4\beta}{24}(w')^2 = (V^2 - \beta)\frac{w^2}{2} - \phi(w).$$

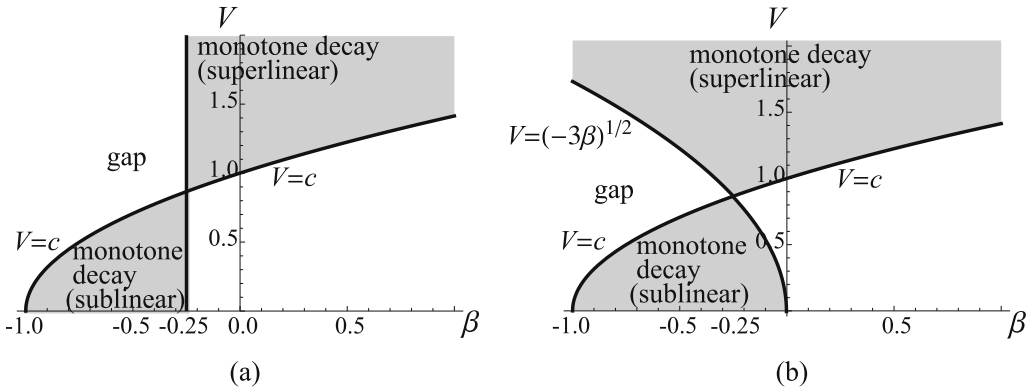

Fig. 15. Velocity ranges where solitary waves may exist for (a) the Boussinesq model (59) and (b) the Collins–Rosenau model (64). See the text for details.

For the cubic potential $\phi(w) = \frac{w^2}{2} + a\frac{w^3}{3}$ this results in [8]

$$w(x) = \frac{3}{2a}(V^2 - c^2)\mathrm{sech}^2\left(\sqrt{\frac{3(V^2-c^2)}{1+4\beta}}x\right),$$

which yields, in agreement with Fig. 15(a), supersonic solutions at $\beta > -1/4$ and $a > 0$ and subsonic ones at $-1 < \beta < -1/4$ and $a < 0$, with both types of solutions monotonically decaying at infinity and delocalizing to zero strain when the sonic limit is approached. At $\beta \to -1/4$ the solutions tend to $w(x) \equiv 0$.

Another low-order quasicontinuum model extends the approximation proposed by Collins [40] and Rosenau [41] by including second-neighbor interactions [8,42]. Following [8], we obtain this model by first rewriting the advance-delay differential equation (4) in Fourier space:

$$\Omega(k)W(k) = F(k), \tag{61}$$

where $W(k)$ and $F(k)$ are the Fourier transforms of $w(x)$ and $f(w(x))$, respectively, and

$$\Omega(k) = \frac{V^2k^2 - \beta\sin^2 k}{4\sin^2(k/2)}, \tag{62}$$

and then expanding $\Omega(k)$ in Taylor series about $k = 0$ (the long-wave limit):

$$\Omega(k) = V^2 - \beta + \frac{1}{12}(3\beta + V^2)k^2 + \frac{1}{240}(V^2 - 5\beta)k^4 + O(k^6) \tag{63}$$

If only $O(k^2)$ terms are retained in the expansion, as in [8], we obtain the following quasicontinuum approximation of the traveling wave equation:

$$-\frac{1}{12}(3\beta + V^2)w'' + (V^2 - \beta)w = f(w). \tag{64}$$

The corresponding partial differential equation for the continuum displacement is

$$u_{tt} = (f(u_y) + \beta u_y)_y + \frac{\beta}{4}u_{yyyy} + \frac{1}{12}u_{yytt}. \tag{65}$$

Unlike (58), it includes a mixed space–time fourth-order derivative, which corresponds to what can be interpreted as "microkinetic" energy term [43]. Similar to (58), it contains a fourth-order spatial derivative term (which vanishes in the case $\beta = 0$ studied in [40,41]) associated with the strain-gradient energy contribution. The characteristic equation for (64) linearized about $w = 0$ is

$$V^2 = \frac{c^2 - \frac{\beta}{4}k^2}{1 + \frac{k^2}{12}} \tag{66}$$

and yields, similar to (60), a symmetric pair of either real or purely imaginary roots. As illustrated in Fig. 14 (dotted curves), for real roots (66) results in a curve which is concave at $k = 0$ and monotonically decreases as k grows at $\beta > -1/4$ (Fig. 14(b, c)), convex at $k = 0$ and monotonically increases with k if $-1 < \beta < -1/4$ (Fig. 14(a)) and remains flat if $\beta = -1/4$. For $-1 < \beta \le 0$ we have $V \to \sqrt{-3\beta}$ as $k \to \infty$. Thus, at $\beta > 0$ the model predicts only supersonic solitary waves. At $-1/4 < \beta < 0$ the waves can be either strictly subsonic, with $V < \sqrt{-3\beta} < c$, or supersonic, $V > c$. Finally, at $-1 < \beta < -1/4$ one can have either subsonic waves, $V < c$, or strictly supersonic, with $V > \sqrt{-3\beta} > c$. In the last two cases subsonic and supersonic waves involve superlinear and sublinear sides of $f(w)$, respectively, and no waves may exist with velocities in the gaps between the curves $V = c$ and $V = \sqrt{-3\beta}$. Note that this quasicontinuum approximation is somewhat closer to the discrete model than the Boussinesq approximation (59), in that it captures the possibility of strictly supersonic solutions (with $V_m = \sqrt{-3\beta}$) and the finite velocity gap at $-1 < \beta < -1/4$, as can be seen by comparing Figs. 15(b) and 2(b). However, the model also predicts strictly subsonic waves at $-1/4 < \beta < 0$, which are not present in either discrete or Boussinesq models. Similar to the Boussinesq model, the decay of the solitary waves at infinity is monotone, since the roots of (66) are purely imaginary.

Again, (64) may also be solved in quadratures, and for the cubic potential one obtains [8]

$$w(x) = \frac{3}{2a}(V^2 - c^2)\mathrm{sech}^2\left(\sqrt{\frac{3(V^2-c^2)}{V^2+3\beta}}x\right),$$

a solitary wave which is subsonic if $a < 0$ and (V, β) is in the lower shaded region in Fig. 15(b) and supersonic if $a > 0$ and (V, β) in the upper shaded region. The waves tend to zero as the velocity bounds $V = c$ and $V = \sqrt{-3\beta}$ are approached.

7.2. Higher-order approximation

The analysis in the previous section shows that the simplest low-order quasicontinuum approximations do a good job at describing the basic features of the diagram in Fig. 2(b) for the discrete model for $\beta \ge 0$, namely, that solitary waves, if they exist for given $f(w)$ in this parameter range, must be supersonic and have monotone decay at infinity. However, these models fail to capture the velocity ranges for existence of solitary waves when $-1 < \beta < 0$, as well as the possibility of oscillatory decay in this parameter regime. An obvious problem with these approximations is that they yield characteristic equations that are of too low order to capture the local maximum of the curve $V(k)$ for real k at $-1 < \beta < -1/4$ and for imaginary k at $-1/4 < \beta < 0$. To obtain these

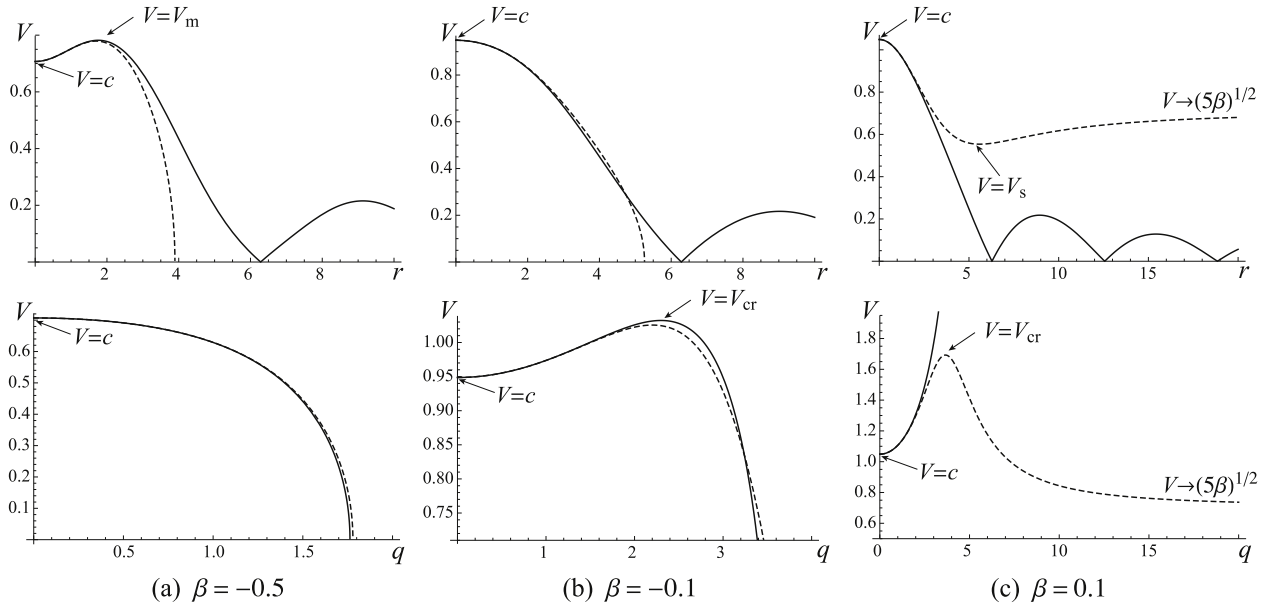

Fig. 16. Real roots $k = r > 0$ and imaginary roots $k = iq$, $q > 0$, of the zero-strain characteristic equations for the quasicontinuum approximation (67) (dashed curves) and the discrete model (solid curves) at (a) $\beta = -0.5$, (b) $\beta = -0.1$ and (c) $\beta = 0.1$.

maxima, it suffices to include the $O(k^4)$ term in the expansion (63), which results in the fourth-order traveling wave equation

$$\frac{1}{240}(V^2 - 5\beta)w'''' - \frac{1}{12}(3\beta + V^2)w'' + (V^2 - \beta)w = f(w). \quad (67)$$

This model, also considered in [42], corresponds to the sixth-order partial differential equation

$$u_{tt} = (f(u_y) + \beta u_y)_y + \frac{\beta}{4}u_{yyyy} + \frac{\beta}{48}u_{yyyyyy} + \frac{1}{12}u_{yytt} - \frac{1}{240}u_{yyyytt}, \quad (68)$$

which includes additional sixth-order spatial and mixed time-spatial derivatives. The characteristic equation for (67) linearized about $w = 0$ is

$$V^2 = \frac{c^2 - \frac{\beta}{4}k^2 + \frac{\beta}{48}k^4}{1 + \frac{1}{12}k^2 + \frac{1}{240}k^4}. \quad (69)$$

For each $V > 0$, it has four roots given by (C.1) in Appendix C. Depending on V, these roots can be real, $k = \pm r$, imaginary, $k = \pm iq$, or complex, $k = \pm\xi \pm i\eta$. Positive real and imaginary roots are shown in Fig. 16. One can see that similar to the discrete model, at $-1 < \beta < -1/4$ real roots exist for velocities below $V_m(\beta) > c$, the maximum of $V(r)$, so solitary waves in this parameter range must be strictly supersonic, $V > V_m$ (see Fig. 16(a)), with complex roots (C.1) governing oscillatory decay at infinity. At $-1/4 < \beta < 0$ real roots exist for $0 \le V \le c$, so the waves must be supersonic. Similar to the discrete model, the curve $V(q)$ for purely imaginary roots $k = \pm iq$ has a maximum $V_{cr}(\beta)$, so that for $c < V < V_{cr}$ there are two symmetric pairs of purely imaginary roots (C.1), and the solution decay is monotone, while above V_{cr} the roots are complex, and the decay is oscillatory. Both $V_m(\beta)$ and $V_{cr}(\beta)$ have the form

$$\hat{V}(\beta) = \sqrt{\frac{6 + 51\beta + 2\sqrt{3}\sqrt{3 + 16\beta + 208\beta^2}}{7}}, \quad (70)$$

where $\hat{V} = V_m$ for $-1 < \beta \le -1/4$ and $\hat{V} = V_{cr}$ for $\beta \ge -1/4$; they coincide at $\beta = -1/4$ ($V_m = V_{cr} = c$), and $V_{cr}(\beta)$ continues into $\beta > 0$ region. These critical velocities are quasicontinuum analogs of the ones defined in (10) and (13) for the discrete model. Quantitative agreement with the discrete model is observed for $-0.45 < \beta < -0.1$, as shown in Fig. 17. Outside this interval the curves $V_m(\beta)$ and $V_{cr}(\beta)$ generated by the discrete model and the approximation (67) diverge since the corresponding values of k_m and q_{cr} at which the maxima occur are outside the interval where the Taylor expansion works well. In particular, the quasicontinuum model predicts a finite value of V_{cr} at $\beta = 0$, with the curve continuing on at $\beta > 0$, while in the discrete case this value tends to infinity as $\beta \to 0$. But overall the approximation captures the main features of the discrete model for $-1 < \beta < 0$ quite well, as can be seen by comparing Fig. 2(b) with Fig. 17 in this parameter regime.

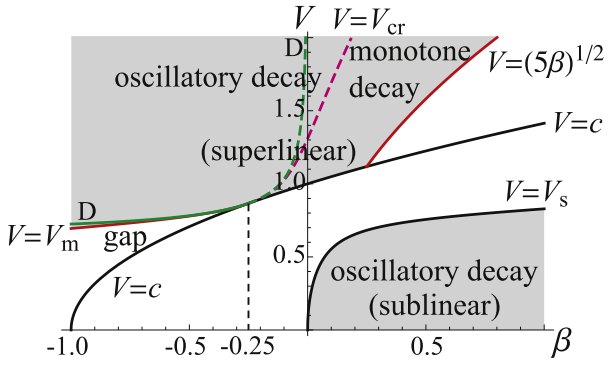

Fig. 17. Velocity ranges where solitary waves may exist for the quasicontinuum model (67). Green curves marked by D show the $V_m(\beta)$ (solid) and $V_{cr}(\beta)$ (dashed) for the discrete model. See the text for details.

However, at $\beta \ge 0$ the higher-order approximation is actually worse than the Boussinesq and Collins–Rosenau models. First, in this parameter regime it predicts the existence of strictly subsonic waves (for sublinear $f(w)$) with $0 < V < V_s(\beta) < c$, where

$$V_s(\beta) = \sqrt{\frac{6 + 51\beta - 2\sqrt{3}\sqrt{3 + 16\beta + 208\beta^2}}{7}} \quad (71)$$

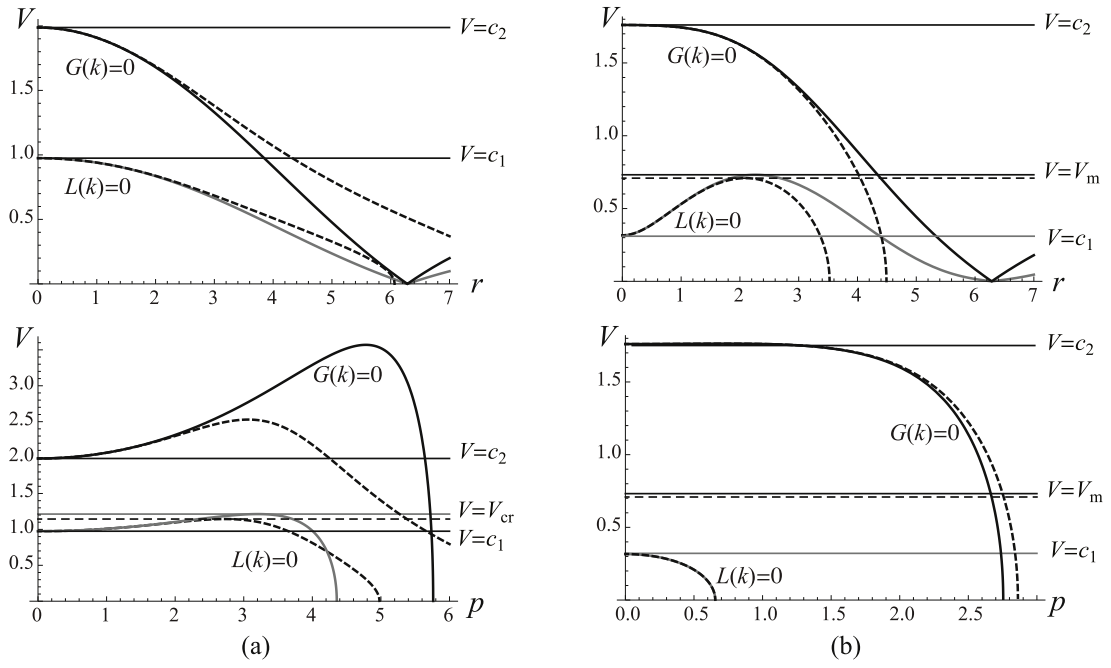

Fig. 18. Real, $k = r > 0$, and imaginary, $k = ip$, $p > 0$, roots of the characteristic equations in the two linear regimes for the discrete model (solid curves, black for $G(k) = 0$, gray for $L(k) = 0$) and its quasicontinuum approximation (67) (thick dashed curves) at $\alpha = 4$ and (a) $\beta = -0.05$; (b) $\beta = -0.9$. For $V = V_{cr}$ and $V = V_m$, the solid horizontal line indicates the value for the discrete model, while the dashed line below is its quasicontinuum approximation.

corresponds to the local minimum of the $V(r)$ curve (see the top panel in Fig. 16(c)), and oscillatory decay at infinity. Recall for both discrete model and the approximations (59) and (64) the waves can be only supersonic in this parameter range. Second, while it also allows supersonic waves (for superlinear $f(w)$), at $\beta > 1/4$ such waves must be strictly supersonic, with $V > \sqrt{5\beta} > c$. Moreover, supersonic waves with $V > V_{cr}(\beta)$ have an oscillatory decay, while the decay is strictly monotone in both discrete model and its two lower order approximations. Clearly, these significant discrepancies are artifacts of the polynomial expansion (63) at $\beta \geq 0$, which, while faithful to the discrete model at small wave numbers (long-wave limit) produces at larger k the features not present in the characteristic equation for the discrete model. For the lower-order approximations, similar artifacts take place when $-1 < \beta < 0$ and are responsible for prediction of subsonic solutions not present in the discrete model.

These results illustrate that quasicontinuum models do not always even qualitatively reflect important features of the discrete model and are applicable only in certain parameter regimes. In this case, the lower-order models (59) and (64) may be used for $\beta \geq 0$, while a higher-order approximation such as (67) is clearly needed when $-1 < \beta < 0$.

Piecewise linear NN interactions. We now use the quasicontinuum model (67) at $-1 < \beta < 0$ with the piecewise linear NN interaction force (14) and compare the ensuing solitary waves with those obtained above for the discrete model. In this case the characteristic equation for (67) in the first linear regime (analog of $L(k) = 0$ in the discrete model) is given by (69) with $c = c_1$. The corresponding analog of $G(k) = 0$ for the second linear regime is (69) with $c = c_2$. Here we recall (15). Real and purely imaginary roots of the characteristic equations for the quasicontinuum and discrete model in the two linear regimes, along with the corresponding critical velocities V_m and V_{cr} defined in (70) are shown in Fig. 18. As described above, in the first regime we have four purely imaginary roots $k = \pm iq_1$ and $k = \pm iq_2$ for $c_1 < V < V_{cr}$ when $-1/4 < \beta < 0$ and four complex roots $k = \pm\xi \pm i\eta$ for $V_{cr} < V < c_2$ when $-1/4 < \beta < 0$ and for $V_m < V < c_2$ when $-1 < \beta < -1/4$; all of these roots are given by (C.1) in Appendix C. Note that due its poor prediction of V_{cr} (much lower than the actual value) for sufficiently small $\beta \leq 0$, the quasicontinuum model (67) yields complex roots with nonzero real part in the first linear regime, and hence decaying oscillations at infinity, at some velocities for which the discrete model has purely imaginary roots of $L(k) = 0$ near the origin. Meanwhile, in the second linear regime, there are purely imaginary roots $k = \pm ip$ and real roots $k = \pm r$ in the corresponding velocity intervals. These roots are given by (C.2) in Appendix C.

Using the roots of the characteristic equations, we construct the solitary wave solution of (67) with $f(w)$ given by (14); see Appendix C for details. At $c_1 < V < V_{cr}$ and $-1/4 < \beta < 0$, we obtain

$$w(x) = w_c \times \begin{cases} \dfrac{\alpha - 1}{c_2^2 - V^2} + D_1 \cos(rx) + D_2 \cosh(px), & |x| \leq z, \\ C_1 \exp(-q_1|x|) + C_2 \exp(-q_2|x|), & |x| \geq z, \end{cases} \tag{72}$$

where the coefficients are given by (C.3), and z is the smallest positive root of the nonlinear equation

$$\begin{aligned} &p\cosh(pz)[(q_1+q_2)r(p^2+r^2)\cos(rz) \\ &+ (q_1q_2(q_1^2+q_1q_2+q_2^2)+2q_1q_2r^2-r^4)\sin(rz)] \\ &+ \sinh(pz)[(p^4+2p^2q_1q_2-q_1q_2(q_1^2+q_1q_2+q_2^2))r\cos(rz) \\ &+ q_1q_2(q_1+q_2)(p^2+r^2)\sin(rz)] = 0. \end{aligned} \tag{73}$$

As in the $n = 2$ approximation considered above, one can show that such z exists.

For $V_{cr} < V < c_2$, $-1/4 < \beta < 0$ and $V_m < V < c_2$, $-1 < \beta < -1/4$, the solution is given by

$$w(x) = w_c \times \begin{cases} \dfrac{\alpha - 1}{c_2^2 - V^2} + D_1 \cos(rx) + D_2 \cosh(px), & |x| \le z, \\ \exp(-\eta|x|)(C_1 \cos(\xi|x|) + C_2 \sin(\xi|x|)), & |x| \ge z, \end{cases} \tag{74}$$

with the coefficients (C.4) and z given by the smallest positive root (whose existence can again be shown) of

$$\begin{aligned} &\cosh(pz)[2\eta pr(p^2 + r^2)\cos(rz) \\ &+ p(3\eta^4 - (r^2 - \xi^2)^2 + 2\eta^2(r^2 + \xi^2))\sin(rz)] \\ &+ \sinh(pz)[r(-3\eta^4 + 2\eta^2(p^2 - \xi^2) + (p^2 + \xi^2)^2)\cos(rz) \\ &+ 2\eta(p^2 + r^2)(\eta^2 + \xi^2)\sin(rz)] = 0. \end{aligned} \tag{75}$$

Figs. 19 and 20 compare $z(V)$ and amplitude–velocity curves obtained using the quasicontinuum approximation to those for the discrete model and its $n = 2$ approximation for $\beta = -0.2$ and $\beta = -0.4$, respectively (with $\alpha = 4$ and $w_c = 1$). As one can see from Fig. 17, at these values of β, the quasicontinuum model predicts V_m and V_{cr} that are close to the actual values, although slightly smaller. The resulting $z(V)$ and amplitude–velocity curves are also quite close to the ones for the discrete model, particularly at smaller velocities where they are even closer than the values obtained from the $n = 2$ approximation. However, in the overall velocity ranges the $n = 2$ approximation clearly does a better job of capturing solutions of the discrete problem, as can be seen in the $z(V)$ plots and insets in the amplitude–velocity plots showing the amplitude differences. This is due to the fact that the quasicontinuum model is based on the expansion around $k = 0$, and thus can never approximate the first nonzero roots of $L(k) = 0$ and $G(k) = 0$ equally well, while the $n = 2$ model involves the exact roots. Note also that the quasicontinuum approximation predicts higher amplitudes and generally lower z values (except for a narrow velocity range near V_m in Fig. 20a) than the discrete model.

Importantly, the quasicontinuum model captures the behavior near the lower velocity limit V_m at $-1 < \beta < -1/4$ (although, as shown in Fig. 17, it significantly underestimates V_m for β closer to -1). As in the $n = 2$ model, in this limit $z \to 0$, $\eta \to 0$, and the solution approaches the linear cosine wave $w(x) = w_c \cos(k_m x)$, similar to Fig. 7, where k_m is the limit of ξ for the quasicontinuum approximation. Meanwhile, in the limit $V \to c_1$ at $-1/4 < \beta < 0$, we have $q_1 \to 0$, while all roots tend to finite values. This implies that (73) yields a finite value of z in this limit, and we have $C_1 \to 1$, while all other coefficients tend to zero in (72), yielding $w(x) \equiv w_c$ as the limiting solution, as before.

Analysis of the solution in the upper sonic limit $V \to c_2$ also yields results mimicking the ones obtained for the $n = 2$ approximation. When $\alpha > -4\beta$, the amplitude becomes infinite in this limit, with the same asymptotic behavior as in (54), and $z \to \infty$ as well. When $-1 < \beta < -1/4$ and $\alpha < -4\beta < 1$, both have finite limits.

8. Smooth NN interactions and higher-order NLS equation

The piecewise linearity of our model brings analytic transparency but carries with it important drawbacks. For instance, the bifurcations of solitary waves from the homogeneous configuration for $\beta \ge -1/4$ (at the sonic velocities) and from the periodic configurations for $-1 < \beta < -1/4$ (at supersonic velocities) are not described properly: in both cases the solitary wave has a finite amplitude as it approaches the bifurcation point. To capture these bifurcations one has to consider smoother interaction potentials.

To be specific, we consider the simplest polynomial form

$$f(w) = w + aw^2 + bw^3. \tag{76}$$

Recall that solitary waves may exist in this model only in velocity intervals (12). At $\beta \ge -1/4$ bifurcate from the sonic limit $V = c$ with $k = 0$, and we expect solitary waves to be adequately described by the long-wave KdV limit as their velocity approaches c, similarly to the classical FPU case $\beta = 0$ [4]. Meanwhile, strictly supersonic lattice waves at $-1 < \beta < -1/4$ bifurcate from the short-length linear wave with $V = V_m > c$ and $k = k_m > 0$ satisfying (11). Below we focus on this bifurcation, which, to the best of our knowledge, has not been previously described for lattice solitary waves.

Our analysis is inspired by the earlier work on solitary wave solutions of partial differential equations modeling capillary–gravity water waves [13–16], where a similar bifurcation (in that case, from a minimum phase velocity) takes place. Those models were based on fifth-order KdV and Euler equations, and the authors obtained the lowest-order description of these waves by deriving the associated nonlinear Schrödinger (NLS) equation for the amplitude of slowly modulated wave packet. The previous work revealed that to approximate *steady* solitary wave solutions in these models, higher-order corrections to the NLS equation must be included [15,16]. Accounting for such higher-order effects allows one to obtain the leading-order approximation of solitary waves bifurcating from the nontrivial configuration where group and phase velocities coincide [15]. Below we adapt this approach to our lattice problem.

Modulation equation. We seek small-amplitude solutions of (3) with $f(w)$ given by (76) in the form of modulated plane-wave packet

$$\begin{aligned} w_n(t) = {} & \varepsilon A(X, T, \tau)e^{i\psi} + \varepsilon^2(B_0(X, T, \tau) + B_2(X, T, \tau)e^{2i\psi}) \\ & + \text{c.c.} + O(\varepsilon^3), \end{aligned} \tag{77}$$

where $\varepsilon \ll 1$, c.c. denotes the complex conjugate, and we set

$$X = \varepsilon n, \quad T = \varepsilon t, \quad \tau = \varepsilon^2 t, \quad \psi = k_m n - \omega_m t.$$

Here X, T and τ define space and time scales, and ψ is the phase variable with wave number $k_m > 0$ and frequency $\omega_m = \omega(k_m)$ satisfying the dispersion relation (8) and the condition (11). The ansatz (77) is equivalent to the one considered in [15] with the obvious modifications for the discrete problem [6,44,45]. It accounts for the formation of higher-order harmonics due to nonlinearity of $f(w)$. As in [15], the $O(\varepsilon^2 e^{i\psi})$ term is not included, since it turns out that it is not determined at the order of multiple-scale expansion considered here and thus can be set to zero from the outset.

Substituting (77) into (3) and collecting the terms up to $O(\varepsilon^3)$ (see Appendix D for details), one can show that the amplitude of the leading-order term has the form

$$A = A(\zeta, \tau), \quad \zeta = X - V_m T \tag{78}$$

and satisfies the NLS equation

$$A_\tau + i\lambda A_{\zeta\zeta} + i\mu|A|^2 A = 0, \tag{79}$$

where

$$\lambda = -\frac{1}{2}\omega''(k_m) \tag{80}$$

and

$$\mu = \frac{2\sin^2\frac{k_m}{2}}{\omega_m}\left\{3b + \frac{8a^2\sin^2 k_m}{4\omega_m^2 - \omega^2(2k_m)} + \frac{4a^2}{V_m^2 - c^2}\right\}. \tag{81}$$

At $\beta = 0$ (79) reduces to the NLS equation for the classical FPU problem [45]. Here we recall that V_m in (78) is defined in (10).

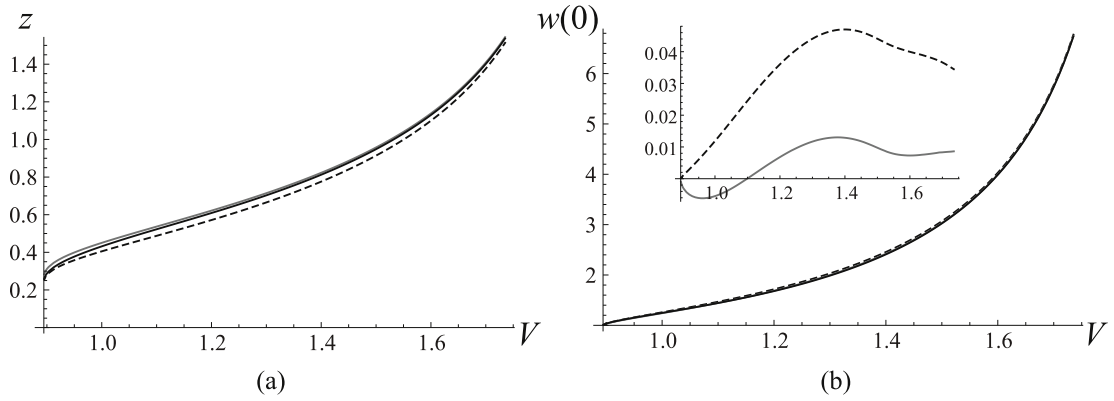

Fig. 19. Comparison of (a) the relation $z(V)$ and (b) the corresponding amplitude–velocity relation at $\alpha = 4$, $\beta = -0.2$ and $w_c = 1$ obtained from the semi-analytical solution (solid black curves), its $n = 2$ approximation (gray curves) and the quasicontinuum model (67) (dashed curves). Inset in (b) shows the amplitude difference from the semi-analytical solution for the $n = 2$ (gray curve) and quasicontinuum (dashed curve) approximations.

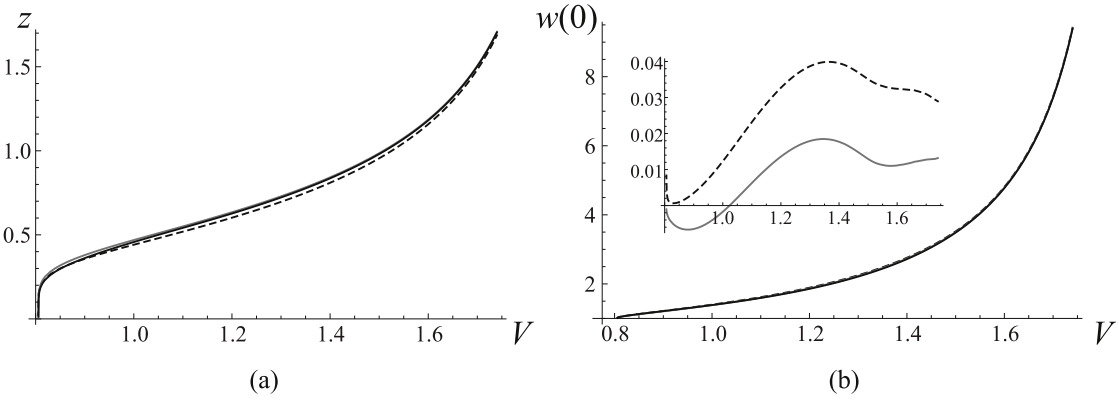

Fig. 20. Comparison of (a) the relation $z(V)$ and (b) the corresponding amplitude–velocity relation at $\alpha = 4$, $\beta = -0.4$ and $w_c = 1$ obtained from the semi-analytical solution (solid black curves), its $n = 2$ approximation (gray curves) and the quasicontinuum model (67) (dashed curves). Inset in (b) shows the amplitude difference from the semi-analytical solution for the $n = 2$ (gray curve) and quasicontinuum (dashed curve) approximations.

To get the higher-order correction to (79) necessary to construct a steady solitary wave, we need to consider $O(\varepsilon^4)$ terms in the expansion. This yields

$$A_\tau + i\lambda A_{\zeta\zeta} + i\mu|A|^2A + \varepsilon\left\{\nu|A|^2A_\zeta + \kappa(|A|^2A_\zeta - A^2\bar{A}_\zeta) + \rho A_{\zeta\zeta\zeta} - \frac{\mu}{k_m}(|A|^2A)_\zeta\right\} = 0, \tag{82}$$

where the coefficients in front of higher-order terms are given by

$$\rho = -\frac{1}{6}\omega'''(k_m), \tag{83}$$

$$\nu = \frac{\sin k_m}{\omega_m}\left\{4a^2\left[\frac{3}{V_m^2 - c^2} + \frac{1 + 4\cos k_m - 5\cos 2k_m}{4\omega_m^2 - \omega^2(2k_m)} - \frac{64\sin^2 k_m \sin^4\frac{k_m}{2}(1 + \beta + 2\beta\cos k_m + \beta\cos 2k_m)}{(4\omega_m^2 - \omega^2(2k_m))^2}\right] + 9b\right\} \tag{84}$$

and

$$\kappa = -\frac{\sin k_m}{\omega_m}\left\{4a^2\left(\frac{1}{V_m^2 - c^2} + \frac{2\sin^2 k_m}{4\omega_m^2 - \omega^2(2k_m)}\right) + 3b\right\}. \tag{85}$$

Leading-order approximation. Following [15], we now seek solution of (82) in the form

$$A = R(\chi)\exp[i\varepsilon\varphi(\chi) + i\varepsilon l\chi - i\sigma\tau], \quad \chi = \zeta - \varepsilon v\tau, \tag{86}$$

with the functions $R(\chi)$, $\varphi(\chi)$ and parameters l, σ and v to be determined. We further require that

$$\sigma = vk_m, \tag{87}$$

which ensures [15] that the total phase of the leading-order approximation,

$$w_n^A(t) = 2\varepsilon\mathrm{Re}[Ae^{ik_m(n - V_m t)}] = 2\varepsilon R(\chi) \times \cos\left[k_m\left(\frac{\chi}{\varepsilon} + v\tau\right) + \varepsilon\varphi(\chi) + \varepsilon l\chi - \sigma\tau\right], \tag{88}$$

depends only on $\chi = \varepsilon(n - (V_m + v\varepsilon^2)t)$:

$$k_m\left(\frac{\chi}{\varepsilon} + v\tau\right) + \varepsilon\varphi(\chi) + \varepsilon l\chi - \sigma\tau = \frac{k_m\chi}{\varepsilon} + \varepsilon(\varphi(\chi) + l\chi).$$

Since its amplitude also depends on χ, the entire approximation (88) is a function of χ, or, equivalently, a traveling solitary wave depending on $x = \chi/\varepsilon = n - Vt$, with velocity

$$V = V_m + v\varepsilon^2. \tag{89}$$

Substituting (86) in (82) yields, up to $O(\varepsilon^2)$ terms,

$$\lambda R'' - \sigma R + \mu R^3 = 0 \tag{90}$$

and

$$-[v+2\lambda(l+\varphi')]R'-\lambda R\varphi''+\rho R'''+\left(v-\frac{3\mu}{k_{\rm m}}\right)R^2R'=0. \quad (91)$$

Note that λ defined in (80) is positive, and one can verify that for $b\geq 0$ and $-1<\beta<-1/4$ (the parameter range of interest), we have $\mu>0$ in (81). Thus, $\lambda\mu>0$, and we are dealing with the so-called focusing NLS equation (with higher-order corrections). In this case Eq. (90) has solution in the form

$$R(\chi)=R_0\,\mathrm{sech}(\gamma\chi), \quad (92)$$

with

$$\sigma=\lambda\gamma^2,\quad R_0^2=\frac{2\lambda\gamma^2}{\mu},\quad v=\frac{\lambda\gamma^2}{k_{\rm m}}, \quad (93)$$

where we used (87) to obtain the last equality. Since λ and μ are both positive, this defines a real R_0 in (92), and we have $\sigma>0$ and $v>0$, with the last inequality meaning that the wave velocity (89) increases away from the bifurcation value $V_{\rm m}$ with ε. As shown in the Appendix D, solving (91) and using (92) then yields

$$l=\frac{\gamma^2}{2}\left(\frac{\rho}{\lambda}-\frac{1}{k_{\rm m}}\right), \quad (94)$$

and

$$\varphi(\chi)=\frac{R_0^2}{4\gamma\lambda}\left\{v-3\mu\left(\frac{1}{k_{\rm m}}+\frac{\rho}{\lambda}\right)\right\}\tanh(\gamma\chi). \quad (95)$$

Substituting (92), (93), (95) and (94) into (88) and the last equality in (93) into (89), we obtain the following leading-order approximation of the solitary wave solution bifurcating from the maximum of the dispersion curve at $-1<\beta<-1/4$:

$$\begin{aligned} w_n^A(t)&=2\sqrt{\frac{2\lambda}{\mu}}(\gamma\varepsilon)\mathrm{sech}(\gamma\varepsilon x)\\ &\times\cos\left[\left\{k_{\rm m}+\frac{(\gamma\varepsilon)^2}{2}\left(\frac{\rho}{\lambda}-\frac{1}{k_{\rm m}}\right)\right\}x\right.\\ &\left.+\frac{\gamma\varepsilon}{2}\left\{\frac{v}{\mu}-3\left(\frac{1}{k_{\rm m}}+\frac{\rho}{\lambda}\right)\right\}\tanh(\gamma\varepsilon x)\right],\quad x=n-Vt,\\ V&=V_{\rm m}+\frac{\lambda}{k_{\rm m}}(\gamma\varepsilon)^2. \end{aligned} \quad (96)$$

Observe that for given $k_{\rm m}$, which determines $V_{\rm m}$, λ, μ, v and ρ, the solution (96) depends only on the single effective parameter $\gamma\varepsilon$, which can be expressed in terms of wave velocity for given $V\geq V_{\rm m}$:

$$\gamma\varepsilon=\sqrt{\frac{(V-V_{\rm m})k_{\rm m}}{\lambda}}. \quad (97)$$

Thus, (96) completely determines the leading approximation of the solitary wave with given velocity near $V_{\rm m}$. We remark that it describes oscillations of period $2\pi/k_{\rm m}+O(V-V_{\rm m})$ that decay on the scale of $O((V-V_{\rm m})^{-1/2})$. Typical strain profiles generated by the approximation (96) are shown in Fig. 21.

Note that the approximation (96) yields the square-root amplitude–velocity relation

$$w(0)=2\sqrt{\frac{2(V-V_{\rm m})k_{\rm m}}{\mu}}, \quad (98)$$

which depends on the parameters of the nonlinearity only through μ in (81). The relation (98) is illustrated in Fig. 22 for different parameters.

Numerical illustrations. We now proceed to solve (4) numerically to generate a family of solitary waves bifurcating from $V_{\rm m}$. To this end, we adopt the numerical codes in [37], where the Fourier spectral collocation method and continuation procedure used in [46] for the regular FPU problem were extended to the problem with long-range interactions. First, observe that assuming $w(x)=o(1/x)$, $w'(x)=o(1/x^2)$, multiplying (4) by x^2 and integrating it over the real line, we obtain

$$(V^2-\beta)\int_{-\infty}^{\infty}w(x)dx=\int_{-\infty}^{\infty}f(w(x))dx. \quad (99)$$

As in [46], this identity is used in the numerical procedure to impose the constraint that the solutions vanish at infinity. Following [46,37], we assume L-periodic solutions with a large even period L and discretize (4) on the finite interval $(-L/2,L/2]$ with mesh step Δx such that $1/\Delta x$ is an integer, so that the advance and delay terms are well defined on the mesh. We also obtain a trapezoidal approximation of (99) with the same mesh. The resulting system is solved using a Fourier collocation method as in [37] for an initial velocity slightly above $V_{\rm m}$ using (96) at velocity close to (but above) $V_{\rm m}$ as an initial guess. A continuation procedure is then employed to compute solutions at larger velocities, with solution at the previous step used as an initial guess to obtain solution at the current step.

As an example, we consider the case $\beta=-0.6$, $a=1$, $b=0$ (quadratic nonlinearity). Fig. 23(a) shows the leading-order approximation (96) (red curve) at the initial velocity $V=0.7684$ slightly above the bifurcation value $V_{\rm m}=0.7645$ used as an initial guess to compute the numerical solution shown in black. We used $\Delta x=0.1$ and $L=400$ in the simulation. Note that the numerical solution has a larger amplitude but the approximation captures well its main features.

Solutions at larger velocities are shown in Fig. 24. Observe that as the velocity increases away from the bifurcation value, solutions gradually lose their envelope-soliton character while still retaining decaying amplitude oscillations in their tails. Fig. 23(b) compares the resulting amplitude–velocity relation to the corresponding relation (98) for the approximation. One can see that the approximation captures the relation well at small velocities close to the bifurcation point (while underestimating the amplitude) but clearly is no longer valid at larger velocities.

We tested the stability of the obtained solitary waves by numerically solving (3) with initial conditions obtained from a wave with given velocity. As illustrated in Figs. 25 and 26, the resulting steady propagation of such waves along the lattice suggests their stability.

9. Conclusions

It is usually assumed that weak solitary waves in lattices are necessarily near-sonic, that they spread over many inter-particle distances and can be therefore described by the low-order, long-wave quasicontinuum approximations exemplified by the KdV equation. Here we have shown that this intuitive picture holds only for lattices with 'ferromagnetic' interactions described by convex inter-particle potentials. More precisely, if in addition to such stabilizing interactions, the model also contains sufficiently strong destabilizing 'anti-ferromagnetic' interactions, described by concave potentials, the character of the weak solitary waves changes and they take the form of long-wave envelopes modulating underlying lattice-scale oscillations. While being supersonic, such solutions cannot reach the conventional sonic limit from which they are separated by a finite gap.

We have also shown that the conventional low-order quasicontinuum theories with one internal length scale fail to capture this gap and one needs to use higher-order theories carrying at least two internal length scales. We constructed a family of explicit solutions describing discrete solitary waves in the model with

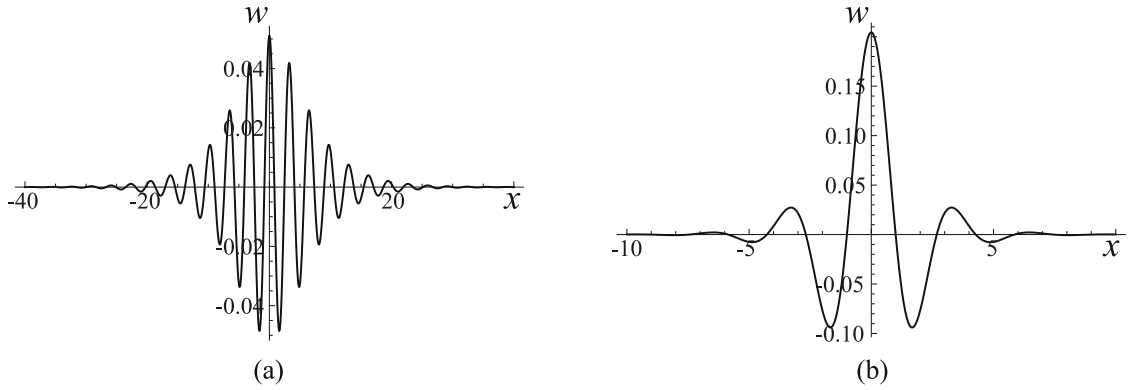

Fig. 21. Approximate solitary wave profiles (96) at (a) $\gamma\varepsilon = 0.2$, (b) $\gamma\varepsilon = 0.8$. Here $\beta = -0.6$, $a = 1$, $b = 0$, which yield $V_{\rm m} = 0.7645$, with $V = 0.7680$ in (a) and $V = 0.8205$ in (b).

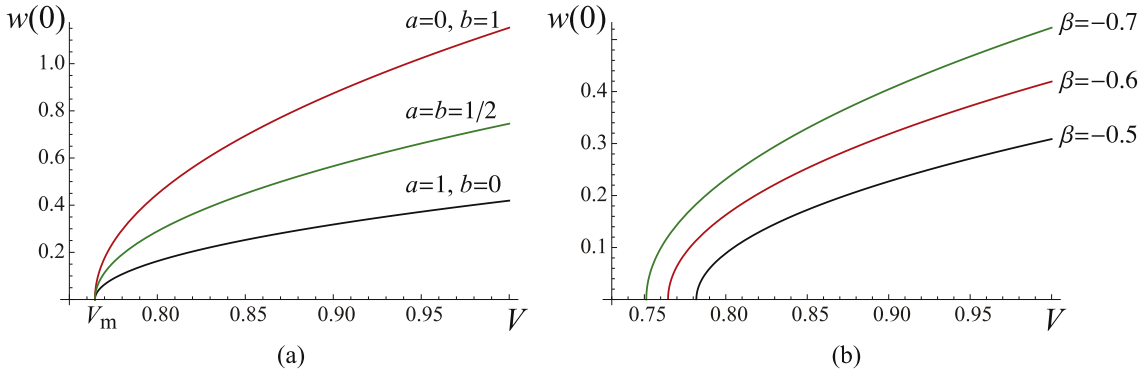

Fig. 22. Amplitude–velocity relation (98) at (a) $\beta = -0.6$, for different a and b; (b) different β at $a = 1$, $b = 0$.

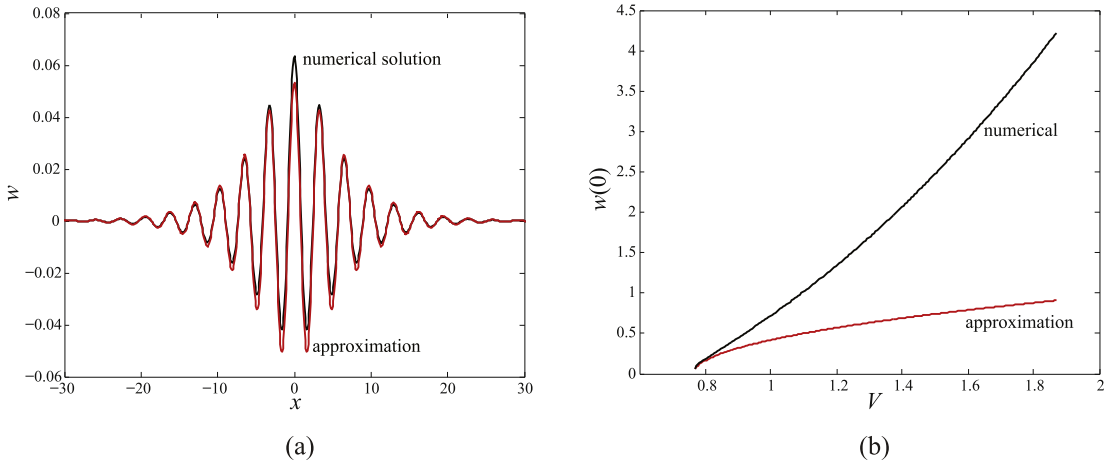

Fig. 23. (a) Numerically computed solitary wave solution (black) at $V = 0.7684$ near the bifurcation point $V_{\rm m} = 0.7645$ and the corresponding approximation (96) (red) used as an initial guess. (b) Amplitude–velocity relation for the numerically computed solitary waves and the corresponding relation (98) providing an approximation near the bifurcation point. Here $\beta = -0.6$, $a = 1$, $b = 0$.

piecewise linear interactions and developed a higher-order quasi-continuum theory reproducing all essential features of such lattice solutions. To describe the fine structure of the bifurcation of weak solitary waves from the linear waves, we went beyond piecewise linear NN interactions and derived an appropriate higher-order NLS equation, which yields the leading-order approximation for the bifurcating solutions in the case of smooth NN potentials. This approximation was then used to numerically compute the strictly supersonic waves that appear to be stable. In particular, this development shows that when β is sufficiently negative, solitary waves become two-scale coherent structures and acquire some features of discrete breathers. As we approach the threshold $\beta = -1/4$ from below, the smaller length scale become irrelevant for weak solitary waves, and the NLS-based description merges with the conventional Boussinesq (KdV) description.

Our work can be also viewed as a cautionary tale about the danger of indiscriminately using quasicontinuum theories based on formal long-wave expansions. Our examples show that such approximations may capture the behavior of the discrete model in a certain parameter range while grossly misrepresenting the essential features of the discrete problem outside this range. In particular, while the low-order approximations we considered are

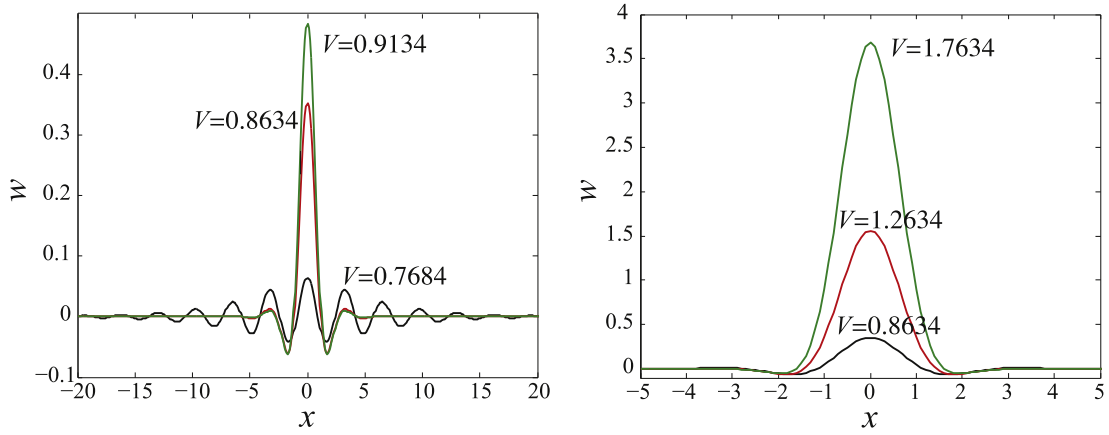

Fig. 24. Numerically computed solitary wave solutions at different velocities. Here $\beta = -0.6$, $a = 1$, $b = 0$.

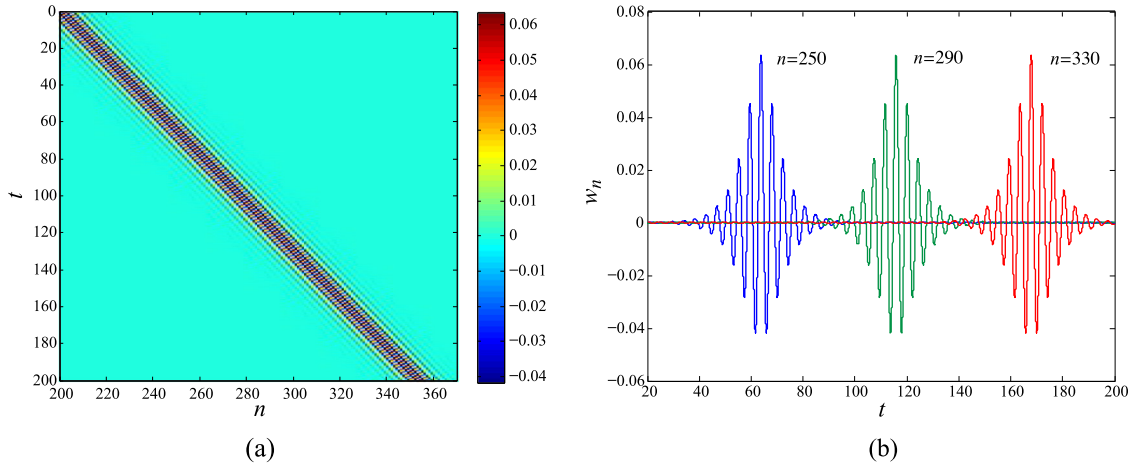

Fig. 25. Results of the numerical simulation of (3) initiated by the computed solitary wave with $V = 0.7684$: (a) space–time evolution of strain $w_n(t)$; (b) strain profiles at some n. Here $\beta = -0.6$, $a = 1$, $b = 0$.

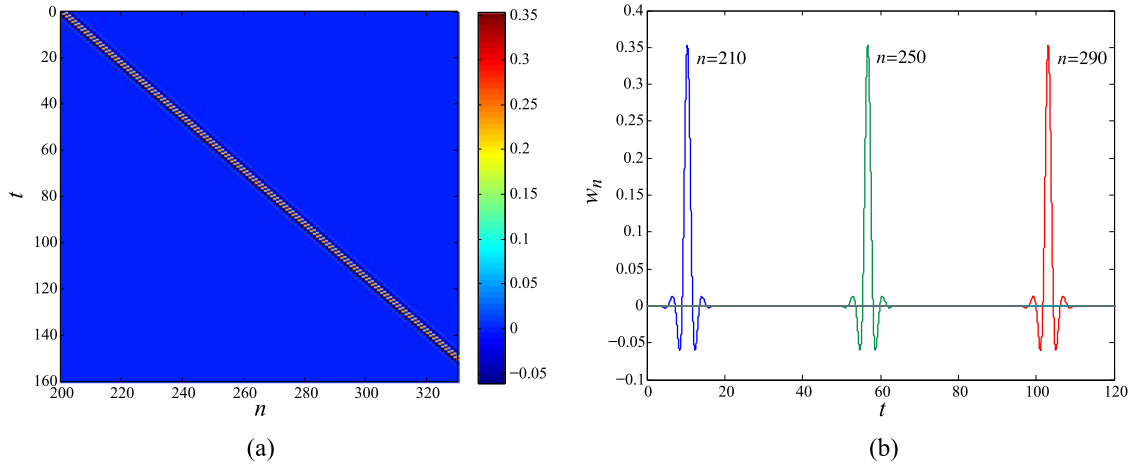

Fig. 26. Results of the numerical simulation of (3) initiated by the computed solitary wave with $V = 0.8634$: (a) space–time evolution of strain $w_n(t)$; (b) strain profiles at some n. Here $\beta = -0.6$, $a = 1$, $b = 0$.

adequate for $\beta \geq 0$, they predict subsonic solitary waves for $-1 < \beta < -1/4$, which prompted some authors [6–8] to assume that such waves exist in the discrete model. We have shown, however, that the discrete model excludes this possibility due to the generic presence of radiation damping at subsonic velocities. Similarly, while the higher-order quasicontinuum model we developed works reasonably well for $-1 < \beta < 0$, the expansion introduces unwanted artifacts for $\beta \geq 0$. These examples remind us that quasicontinuum theories should not be used, even for a qualitative prediction, outside the rigorously established ranges of their validity.

We conclude with an observation that an interesting semantic conundrum is associated with the very definition of a supersonic wave in one-dimensional lattice models. The conventional idea of a sonic velocity links it with the long-wave dispersionless limit of the discrete model. In the classical continuum model such sonic velocity is universal, characterizing the propagation of a general signal. As we have shown, in dispersive models, where waves of different lengths may propagate with different velocities, the conventional long-wave sonic velocity may be lower than the maximal velocity of linear waves. In other words, being supersonic in the conventional sense would not mean being faster than any linear wave. This is exactly the situation we encountered in our problem, where the slowest nonlinear solitary waves are strictly faster than the linear waves with zero wave length but their lowest velocity bound coincides with the phase speed of the fastest linear waves having a finite wave number. These short-length fastest linear waves are the ones for which the group and the phase velocities coincide, the property they share with the infinitely long waves. The velocity of such essentially lattice waves, which are paradoxically supersonic in the conventional sense, may instead serve as an alternative definition of the characteristic (sonic) speed. Under this definition, all of our solitary waves would have a sonic lower velocity bound.

Acknowledgments

The authors thank Jesús Cuevas-Maraver for providing the numerical code which was adapted for simulations described in this work. L.T. was supported by the French Government under the grants ANR-10-IDEX-0001-02 PSL and ANR-17-CE08-0047. A.V. acknowledges support from the U.S. National Science Foundation, under the grant DMS-1506904.

Appendix A. Numerical solution of the integral equation

One can obtain a semianalytical solution of the problem using numerical approximation of the integral equation (23). Since $h(x)$ is odd, it is convenient to rewrite it first in the symmetric form

$$h(x) = (\alpha - 1)\int_0^z K(x,s)h(s)ds, \quad 0 \leq x < z, \tag{A.1}$$

where the kernel is given by

$$K(x,s) = \mathcal{Q}(x+s) - \mathcal{Q}(x-s) = -\frac{2}{\pi(\alpha-1)} \times \int_0^\infty \left(\frac{G(k)}{L(k)} - 1\right)\sin(ks)\sin(kx)dk; \tag{A.2}$$

Note that the function $K(x,s)$ is symmetric. It can be explicitly computed in terms of the roots of (7). Indeed, observe that

$$K(x,s) = 2g(x-s) - 2g(x+s) - g(x-s-1) - g(x-s+1) + g(x+s-1) + g(x+s+1), \tag{A.3}$$

where

$$g(x) = -\frac{1}{2\pi}\int_\Gamma \frac{e^{ikx}}{L(k)}dk.$$

Here the integration contour Γ follows the real axis everywhere except near $k = 0$, where it goes in a small semicircle above the singularity point. Closing the contour by a semicircle in the upper half plane if $x > 0$ and the lower half-plane if $x < 0$, we obtain

$$g(x) = \begin{cases} -i\sum_{i=1}^\infty \dfrac{e^{ix\lambda_i^+}}{L'(\lambda_i^+)}, & x > 0 \\ \dfrac{x}{V^2 - c_1^2} + i\sum_{i=1}^\infty \dfrac{e^{ix\lambda_i^-}}{L'(\lambda_i^-)}, & x < 0. \end{cases} \tag{A.4}$$

Using (A.3) and (A.4) with a sufficiently large number of roots included (typically, $N = 804$), we can accurately compute $K(x,s)$. The integral in the left hand side of the integral equation (A.1) can be then approximated by the trapezoidal rule with a uniform mesh over the interval $[0,z]$, so that the equation is replaced by the linear system $\mathbf{B}(z)\mathbf{h} = \mathbf{h}$, where $\mathbf{B}(z)$ is the matrix replacing the integral operator and $\mathbf{h}$ is the vector representing the unknown shape function at the mesh points. Solving $\det(\mathbf{B}(z) - \mathbf{I}) = 0$, where $\mathbf{I}$ is the identity matrix, we find the value of $z > 0$ that ensures that $\mathbf{B}(z)$ has the eigenvalue $\varrho = 1$, and find the corresponding eigenvector $\mathbf{h}$, normalized using the trapezoidal approximation of (20). The solution is then found using this $\mathbf{h}$ and the trapezoidal approximation of the integral in

$$w(x) = w_c\frac{\int_0^z \mathcal{R}(x,s)h(s)ds}{\int_0^z \mathcal{R}(z,s)h(s)ds}, \tag{A.5}$$

which is obtained from (22) and the condition $w(z) = w_c$, with the kernel

$$\mathcal{R}(x,s) = -\frac{2}{\pi(\alpha-1)}\int_0^\infty \left(\frac{G(k)}{L(k)} - 1\right)\frac{\sin(ks)\cos(kx)}{k}dk \tag{A.6}$$

that is computed similarly to $K(x,s)$. As before, there may be more than one value of z, and we need to discard the spurious solutions that do not satisfy the assumed inequalities. In our calculations, there was always one admissible solution.

To compute the energy (1) of the resulting solution (the Hamiltonian), we will also need the expression for the particle velocity $\dot{u}_n(t) = v(x)$. Observe that $\dot{w}_n = \dot{u}_n - \dot{u}_{n-1}$, and so in the traveling wave coordinates we have $v(x) - v(x-1) = -Vw'(x)$. Solving this equation using the Fourier transform and recalling (22) and (A.5), we obtain

$$v(x) = \frac{Vw_c\int_0^z T(x,s)h(s)ds}{\int_0^z \mathcal{R}(z,s)h(s)ds}, \tag{A.7}$$

where

$$T(x,s) = \frac{1}{\pi(\alpha-1)}\int_0^\infty \left(\frac{G(k)}{L(k)} - 1\right) \times \frac{\sin(ks)\cos(k(x+\frac{1}{2}))}{\sin(k/2)}dk \tag{A.8}$$

is again computed in terms of residues.

Appendix B. Accuracy of the nested approximations

In Section 5 we discussed how the value z_2 and the amplitude $w_2(0)$ of the wave depend on its velocity V. Recall that z_2 solves (40) when $-1/4 < \beta < 0$ and $c_1 < V < V_{\rm cr}$ (monotone decay case) and (47) when either $-1/4 < \beta < 0$ and $V_{\rm cr} < V < c_2$ or $-1 < \beta < -1/4$ and $V_{\rm m} < V < c_2$ (oscillatory decay). Meanwhile, the solution amplitudes are given by (44) and (53), respectively.

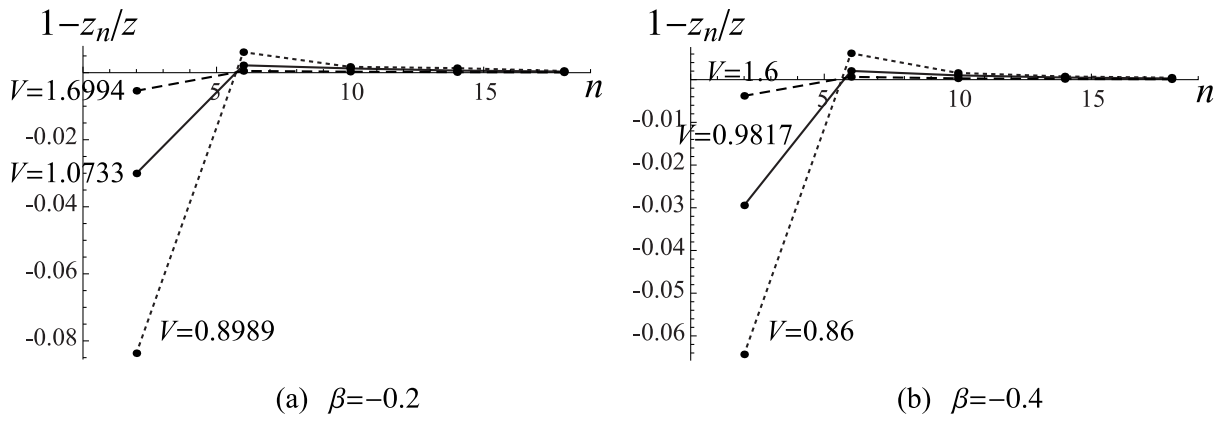

Fig. B.27. The error of the z_n values found by solving (32) relative to the value of z obtained using the trapezoidal approximation of (23). Here $\alpha = 4$ and $w_c = 1$.

In Figs. 19 and 20 we compare the functions $z(V)$ and amplitude–velocity curves generated using the $n = 2$ approximation (gray curves) to the corresponding semi-analytical (black) curves at $\beta = -0.2 \in (-1/4, 0)$ and $\beta = -0.4 \in (-1, -1/4)$, with $\alpha = 4$ and $w_c = 1$. One can see an excellent agreement of the amplitude–velocity curves, which are nearly undistinguishable. The difference between z values is more visible, but the error is still relatively small and decreases at large V.

Importantly, the simplest approximation captures the asymptotic behavior of the curves as velocity approaches the lower and upper limits. In particular, as discussed in Section 5, in the lower sonic limit $V \to c_1$ at $-1/4 < \beta < 0$, the solution delocalizes to a straight line $w(x) = w_c$, so $w(0) \to w_c$, as can be seen in Fig. 19(b), but $z(V)$ approaches a finite nonzero value in this limit, as shown in Fig. 19(a), with the simplest approximation predicting a slightly larger value than the semi-analytical result. As velocity approaches the lower limit, $V \to V_m$, at $1 < \beta < -1/4$, and the solution tends to the linear cosine wave as shown in Fig. 7, we have $z(V) \to 0$, as illustrated in Fig. 20(a), while the amplitude tends to w_c in this limit, as shown in Fig. 20(b). Meanwhile, in the upper velocity limit, $V \to c_2$, we have both $z(V)$ and the amplitude tending to infinity in both cases if $\alpha > -4\beta$ (as in the examples shown), while at $1 < \alpha < -4\beta$, $-1 < \beta < -1/4$ they approach finite values, as discussed in Section 5.

As more roots are included, the accuracy of the approximation rapidly improves. Fast convergence of z_n values obtained by solving (32) at given n is illustrated in Fig. B.27. For both values of β and velocities shown in the figure, the error of the approximation is less than 0.3% for $n \geq 10$.

Appendix C. Some technical results for the quasicontinuum approximation

To construct the solution of (67) with $f(w)$ given by (14), we solve the equation in the first and second linear regimes in terms of the roots of the corresponding characteristic equations. These roots are given by

$$k = \pm\sqrt{\frac{2}{5\beta - V^2}} \times \sqrt{15\beta + 5V^2 \mp \sqrt{5(-60\beta - 15\beta^2 + (12 + 102\beta)V^2 - 7V^4)}} \tag{C.1}$$

and

$$k = \pm\sqrt{\frac{2}{5\beta - V^2}} \times \sqrt{15\beta + 5V^2 \mp \sqrt{5(-60\alpha\beta - 15\beta^2 + (12\alpha + 102\beta)V^2 - 7V^4)}}, \tag{C.2}$$

respectively. We then use the boundary conditions $w(x) \to 0$ as $|x| \to \infty$, continuity of the $w(x)$ and its first three derivatives at $x = \pm z$, the switch condition $w(\pm z) = w_c$ and the fact that the solution must be even to find z and the coefficients involved in the solution. For $c_1 < V < V_{cr}$ and $-1/4 < \beta < 0$, we obtain (72), where the coefficients are given by

$$\begin{aligned}
C_1 &= e^{q_1 z} q_2 (q_1^2 q_2^2 + p^2 r^2)[p(q_2^2 + r^2)\cosh(pz)\sin(rz) \\
&\quad + ((p^2 - q_2^2) r\cos(rz) + q_2(p^2 + r^2)\sin(rz))\sinh(pz)] \\
&\quad /(p(q_2 - q_1) r\Delta(z)) \\
C_2 &= e^{q_2 z} q_1 (q_1^2 q_2^2 + p^2 r^2)[p(q_2^2 + r^2)\cosh(pz)\sin(rz) \\
&\quad + ((p^2 - q_1^2) r\cos(rz) + q_1(p^2 + r^2)\sin(rz))\sinh(pz)] \\
&\quad /(p(q_1 - q_2) r\Delta(z)) \\
D_1 &= q_1 q_2 (q_1^2 q_2^2 + p^2 r^2)[p(q_1 + q_2)\cosh(pz) \\
&\quad + (p^2 + q_1 q_2)\sinh(pz)]/(pr^2\Delta(z)) \\
D_2 &= q_1 q_2 (q_1^2 q_2^2 + p^2 r^2)[r(q_1 + q_2)\cos(rz) \\
&\quad + (q_1 q_2 - r^2)\sin(rz)]/(p^2 r\Delta(z)),
\end{aligned} \tag{C.3}$$

with

$$\begin{aligned}
\Delta(z) &= \cosh(pz)[r(q_1 q_2(r^2 - q_1 q_2) \\
&\quad + p^2(q_1^2 + q_1 q_2 + q_2^2 + r^2))\sin(rz) \\
&\quad - q_1 q_2(q_1 + q_2)(p^2 + r^2)\cos(rz)] + p\sinh(pz) \\
&\quad \times [(q_1 + q_2) r(p^2 + r^2)\sin(rz) \\
&\quad - (q_1 q_2(p^2 + q_1 q_2) + r^2(q_1^2 + q_1 q_2 + q_2^2 - p^2))\cos(rz)],
\end{aligned}$$

and z is the smallest positive root of the nonlinear equation (73).

For $V_{cr} < V < c_2$, $-1/4 < \beta < 0$ and $V_m < V < c_2$, $-1 < \beta < -1/4$, the solution is given by (74) with the coefficients

$$\begin{aligned}
C_1 &= -e^{\eta z}(p^2r^2 + (\eta^2+\xi^2)^2)[p\cosh(pz)\sin(rz)\\
&\times (\xi(3\eta^2 + r^2 - \xi^2)\cos(\xi z)\\
&- \eta(\eta^2 + r^2 - 3\xi^2)\sin(\xi z)) + \sinh(pz)(r\cos(rz)\\
&\times (\xi(p^2 + \xi^2 - 3\eta^2)\cos(\xi z)\\
&+ \eta(\eta^2 - p^2 - 3\xi^2)\sin(\xi z)) + (p^2+r^2)\sin(rz)\\
&\times (2\eta\xi\cos(\xi z) + (\xi^2 - \eta^2)\sin(\xi z)))]/(pr\xi\Delta(z))\\
C_2 &= -e^{\eta z}(p^2r^2 + (\eta^2+\xi^2)^2)[p\cosh(pz)\sin(rz)\\
&\times (\eta(\eta^2 + r^2 - 3\xi^2)\cos(\xi z)\\
&+ \xi(3\eta^2 + r^2 - \xi^2)\sin(\xi z)) + \sinh(pz)(r\cos(rz)\\
&\times (\eta(p^2 + 3\xi^2 - \eta^2)\cos(\xi z)\\
&+ \xi(\xi^2 + p^2 - 3\eta^2)\sin(\xi z)) + (p^2+r^2)\sin(rz)\\
&\times (2\eta\xi\sin(\xi z) + (\eta^2 - \xi^2)\cos(\xi z)))]/(pr\xi\Delta(z))\\
D_1 &= -(\eta^2+\xi^2)(p^2r^2 + (\eta^2+\xi^2)^2)\\
&\times [2\eta p\cosh(pz) + (\eta^2 + p^2 + \xi^2)\sinh(pz)]/(pr^2\Delta(z))\\
D_2 &= -(\eta^2+\xi^2)(p^2r^2 + (\eta^2+\xi^2)^2)\\
&\times [2\eta r\cos(rz) + (\eta^2 - r^2 + \xi^2)\sin(rz)]/(p^2r\Delta(z)),
\end{aligned} \tag{C.4}$$

where

$$\begin{aligned}
\Delta(z) &= \cosh(pz)[2\eta(p^2+r^2)(\eta^2+\xi^2)\cos(rz)\\
&+ r(\eta^4 - \eta^2(3p^2 + r^2 - 2\xi^2)\\
&- (r^2 - \xi^2)(p^2+\xi^2))\sin(rz)]\\
&+ p\sinh(pz)[(\eta^4 - (r^2 - \xi^2)(p^2+\xi^2)\\
&+ \eta^2(p^2 + 3r^2 + 2\xi^2))\cos(rz) - 2\eta r(p^2+r^2)\sin(rz)]
\end{aligned}$$

and z is the smallest positive root of (75).

Appendix D. Derivation of the modulation equation and leading-order solution

In this Appendix, we provide the details of the derivation of the modulation equation (82) and the leading-order solution (96).

Substituting (77) into (3) and collecting the terms involving $e^{i\psi}$, we obtain

$$\begin{aligned}
&\varepsilon A(-\omega_m^2 + 4\sin^2\frac{k_m}{2} + \beta\sin^2 k_m)\\
&+ \varepsilon^2(-2i\omega_m)(A_T + V_m A_X) + \varepsilon^3\{A_{TT} - 2i\omega_m A_\tau\\
&- [V_m^2 + \omega_m\omega''(k_m)]A_{XX} + 4\sin^2\frac{k_m}{2}\\
&\times (3b|A|^2A + 2aB_2\bar{A} + 2a(B_0 + \bar{B}_0)A)\} +\\
&\varepsilon^4\left\{2A_{T\tau} + i\left[V_m\omega''(k_m) + \frac{1}{3}\omega_m\omega'''(k_m)\right]A_{XXX}\right.\\
&- 4i\sin k_m\left[aA_X(B_0 + \bar{B}_0)\right.\\
&+ aA(B_0 + \bar{B}_0)_X + 3b|A|^2A_X + a(B_2)_X\bar{A}\\
&\left.\left.+ aB_2(\bar{A})_X + \frac{3}{2}bA^2(\bar{A})_X\right]\right\} + O(\varepsilon^5) = 0.
\end{aligned} \tag{D.1}$$

Clearly, the $O(\varepsilon)$ term is zero due to the dispersion relation (8), while the $O(\varepsilon^2)$ term implies that $A = A(\zeta, \tau)$, with ζ defined in (78), which also suggests that $B_0 = B_0(\zeta, \tau)$ and $B_2 = B_2(\zeta, \tau)$. The $O(\varepsilon^3)$ term then yields

$$\begin{aligned}
&-2i\omega_m A_\tau - \omega_m\omega''(k_m)A_{\zeta\zeta} + 4\sin^2\frac{k_m}{2}\\
&\times (3b|A|^2A + 2aB_2\bar{A} + 2a(B_0 + \bar{B}_0)A) = 0.
\end{aligned} \tag{D.2}$$

Next, collecting the terms multiplying $e^{2i\psi}$, we obtain

$$\begin{aligned}
&\varepsilon^2\{(\omega^2(2k_m) - 4\omega_m^2)B_2 + 4aA^2\sin^2 k_m\} +\\
&2i\varepsilon^3\{(2\omega_m V_m - \omega(2k_m)\omega'(2k_m))(B_2)_\zeta - 2a\sin(2k_m)AA_\zeta\}\\
&+ O(\varepsilon^4) = 0.
\end{aligned}$$

One can check that the non-resonance condition

$$4\omega^2(k) \neq \omega^2(2k), \tag{D.3}$$

which implies that the phase velocities of the first and second harmonics must differ, holds at $k = k_m$, so the above equation is solved by

$$B_2 = \frac{4aA^2\sin^2 k_m}{4\omega_m^2 - \omega^2(2k_m)} + \varepsilon\delta AA_\zeta, \tag{D.4}$$

with δ given by

$$\delta = 4ia\left\{\frac{4\sin^2 k_m(2\omega_m V_m - \omega(2k_m)\omega'(2k_m))}{(4\omega_m^2 - \omega^2(2k_m))^2} - \frac{\sin 2k_m}{4\omega_m^2 - \omega^2(2k_m)}\right\}. \tag{D.5}$$

Finally, collecting the terms independent of ψ, we obtain

$$\varepsilon^4\{(B_0 + \bar{B}_0)_{\zeta\zeta}(V_m^2 - c^2) - 2a(|A|^2)_{\zeta\zeta}\} + O(\varepsilon^5) = 0,$$

where we recall that $V_m > c$, with c defined in (9). Up to $O(\varepsilon^5)$ this is solved by

$$B_0 + \bar{B}_0 = \frac{2a|A|^2}{V_m^2 - c^2}. \tag{D.6}$$

Substituting (D.4), (D.5) and (D.6) into (D.1), considering $O(\varepsilon^3)$ terms and dividing by $-2i\omega_{\rm m}$, we obtain the NLS equation (79) with coefficients (80) and (81).

To get the higher-order correction to (79), we consider $O(\varepsilon^4)$ terms in (D.1). The linear $O(\varepsilon^4)$ terms are

$$-2V_{\rm m}A_{\tau\zeta}+i\left(V_{\rm m}\omega''(k_{\rm m})+\frac{1}{3}\omega(k_{\rm m})\omega'''(k_{\rm m})\right)A_{\zeta\zeta\zeta}$$
$$=-2i\omega_{\rm m}\left(\rho A_{\zeta\zeta\zeta}-\frac{\mu}{k_{\rm m}}(|A|^2A)_\zeta\right), \tag{D.7}$$

with ρ given by (83). Here we have differentiated (79) to obtain $A_{\tau\zeta}$ and used (11). Substituting (D.4), (D.5) and (D.6) into (D.1), we obtain the nonlinear $O(\varepsilon^4)$ terms:

$$-2i\omega_{\rm m}(\nu|A|^2A_\zeta+\kappa(|A|^2A_\zeta-A^2\bar{A}_\zeta)), \tag{D.8}$$

where ν and κ are given by (84) and (85), respectively. Combining the $O(\varepsilon^4)$ terms (D.7) and (D.8) divided by $-2i\omega_{\rm m}$ with $O(\varepsilon^3)$ NLS equation (79), we obtain the modulation equation (82) with higher-order corrections. This equation coincides with the one obtained in [15] except for the opposite sign in front of the last term on the left hand side.

We now provide some details about the derivation of the leading-order solution (96). To find $\varphi(\chi)$ in (86), we observe that (91) can be rewritten as

$$\frac{\lambda}{R}(R^2\varphi')'=\rho R'''+\left(\nu-\frac{3\mu}{k_{\rm m}}\right)R^2R'-(v+2\lambda l)R'.$$

Substituting $R'''=(-3\mu R^2R'+\sigma R')/\lambda$ implied by (90) into the above equation and multiplying both sides by R, we obtain

$$\lambda(R^2\varphi')'=\frac{\rho}{\lambda}(-3\mu R^3R'+\sigma RR')+\left(\nu-\frac{3\mu}{k_{\rm m}}\right)R^3R'-(v+2\lambda l)RR'.$$

Assuming that $\varphi'(\chi)$ is bounded when $|\chi|\to\infty$ and integrating this equation, we obtain, after multiplying by $2/R^2$,

$$2\lambda\varphi'(\chi)=-(v+2\lambda l)+\sigma\frac{\rho}{\lambda}+\frac{1}{2}\left(\nu-\frac{3\mu}{k_{\rm m}}-\frac{3\mu\rho}{\lambda}\right)R^2.$$

As in [15], we now assume without loss of generality that $\varphi'(\chi)\to 0$ as $|\chi|\to\infty$, which yields (94), where we have used (93), and

$$\varphi'(\chi)=\frac{1}{4\lambda}\left(\nu-\frac{3\mu}{k_{\rm m}}-\frac{3\mu\rho}{\lambda}\right)R^2.$$

Substituting (92) and integrating, we then obtain (95), where we set the constant of integration to zero to get a solution symmetric about $\chi=0$.

References

[1] C. Daraio, V.F. Nesterenko, E.B. Herbold, S. Jin, Tunability of solitary wave properties in one-dimensional strongly nonlinear phononic crystals, Phys. Rev. E 73 (2) (2006) 026610.

[2] E. Fermi, J. Pasta, S. Ulam, Studies of nonlinear problems. Technical Report LA-1940, Los Alamos Scientific Laboratory, 1955.

[3] G. Friesecke, J.A.D. Wattis, Existence theorem for solitary waves on lattices, Comm. Math. Phys. 161 (2) (1994) 391–418.

[4] G. Friesecke, R.L. Pego, Solitary waves on Fermi-Pasta–Ulam lattices: I. Qualitative properties, renormalization and continuum limit, Nonlinearity 12 (1999) 1601–1626.

[5] J.A.D. Wattis, Approximations to solitary waves on lattices, II: Quasicontinuum methods for fast and slow waves, J. Phys. A 26 (1993) 1193–1209.

[6] N. Flytzanis, S. Pnevmatikos, M. Remoissenet, Kink, breather and asymmetric envelope or dark solitons in nonlinear chains. i. monatomic chain, J. Phys. C: Solid State Phys. 18 (24) (1985) 4603–4629.

[7] N. Flytzanis, S. Pnevmatikos, M. Remoissenet, Soliton resonances in atomic nonlinear systems, Physica D 26 (1) (1987) 311–320.

[8] J.A.D. Wattis, Approximations to solitary waves on lattices, III: the monatomic lattice with second-neighbour interactions, J. Phys. A 29 (1996) 8139–8157.

[9] R.D. Mindlin, Second gradient of strain and surface-tension in linear elasticity, Int. J. Solids Struct. 1 (4) (1965) 417–438.

[10] M. Charlotte, L. Truskinovsky, Linear elastic chain with a hyper-pre-stress, J. Mech. Phys. Solids 50 (2) (2002) 217–251.

[11] M. Charlotte, L. Truskinovsky, Towards multi-scale continuum elasticity theory, Contin. Mech. Thermodyn. (2007).

[12] A. Danescu, Exact continuum interpolation of the linear chain with hyper-pre-stress, Int. J. Fract. 202 (2) (2016) 237–244.

[13] T.R. Akylas, Envelope solitons with stationary crests, Phys. Fluids A 5 (4) (1993) 789–791.

[14] M.S. Longuet-Higgins, Capillary–gravity waves of solitary type and envelope solitons on deep water, J. Fluid Mech. 252 (1993) 703–711.

[15] R. Grimshaw, B. Malomed, E. Benilov, Solitary waves with damped oscillatory tails: an analysis of the fifth-order Korteweg–de Vries equation, Physica D 77 (4) (1994) 473–485.

[16] R.H.J. Grimshaw, Envelope solitary waves, in: R.H.J. Grimshaw (Ed.), Solitary Waves in Fluids, WIT press, 2007, pp. 159–179, chapter 7.

[17] L. Truskinovsky, A. Vainchtein, Solitary waves in a nonintegrable Fermi-Pasta–Ulam chain, Phys. Rev. E 90 (4) (2014) 042903.

[18] W. Atkinson, N. Cabrera, Motion of a Frenkel-Kontorova dislocation in a one-dimensional crystal, Phys. Rev. A 138 (3) (1965) 763–766.

[19] A. Carpio, L.L. Bonilla, Oscillatory wave fronts in chains of coupled nonlinear oscillators, Phys. Rev. E 67 (2003) 056621.

[20] O. Kresse, L. Truskinovsky, Lattice friction for crystalline defects: from dislocations to cracks, J. Mech. Phys. Solids 52 (2004) 2521–2543.

[21] L. Truskinovsky, A. Vainchtein, Kinetics of martensitic phase transitions: Lattice model, SIAM J. Appl. Math. 66 (2005) 533–553.

[22] L.I. Slepyan, Models and Phenomena in Fracture Mechanics, Springer-Verlag, New York, 2002.

[23] A. Vainchtein, E.S. Van Vleck, Nucleation and propagation of phase mixtures in a bistable chain, Phys. Rev. B 79 (14) (2009) 144123.

[24] L. Truskinovsky, A. Vainchtein, The origin of nucleation peak in transformational plasticity, J. Mech. Phys. Solids 52 (2004) 1421–1446.

[25] X. Ren, L. Truskinovsky, Finite scale microstructures in nonlocal elasticity, J. Elasticity 59 (1–3) (2000) 319–355.

[26] A. Braides, M.S. Gelli, Continuum limits of discrete systems without convexity hypotheses, Math. Mech. Solids 7 (1) (2002) 41–66.

[27] S. Pagano, R. Paroni, A simple model for phase transitions: from the discrete to the continuum problem, Quart. Appl. Math. 61 (1) (2003) 89–109.

[28] N. Flytzanis, S. Crowley, V. Celli, High velocity dislocation motion and interatomic force law, J. Phys. Chem. Solids 38 (1977) 539–552.

[29] A. Vainchtein, The role of spinodal region in the kinetics of lattice phase transitions, J. Mech. Phys. Solids 58 (2) (2010) 227–240.

[30] A. Vainchtein, Effect of nonlinearity on the steady motion of a twinning dislocation, Physica D 239 (2010) 1170–1179.

[31] M.P. Ganin, On a Fredholm integral equation whose kernel depends on the difference of the arguments, Izv. Vyssh Uchebn. Zaved. Mat. 2 (1963) 31–43.

[32] B.V. Pal'tsev, Expansion in eigenfunctions of integral operators of convolution on a finite interval with kernels whose fourier transforms are rational. "Weakly" nonselfadjoint regular kernels, Math. USSR Izvestija 6 (3) (1972) 587–630.

[33] Ju. I. Ljubarskii, On the convolution operator on a finite interval, Math. USSR Izvestija 11 (3) (1977) 583–611.

[34] E. Trofimov, A. Vainchtein, Kinks vs shocks in a discrete model of displacive phase transitions, Contin. Mech. Thermodyn. 22 (5) (2010) 317–344; Contin. Mech. Thermodyn. 25 (2013) 107–108, Erratum.

[35] S.F. Mingaleev, Y.B. Gaididei, F.G. Mertens, Solitons in anharmonic chains with ultra-long-range interatomic interactions, Phys. Rev. E 61 (2) (2000) R1044–1047.

[36] N.G. Vakhitov, A.A. Kolokolov, Stationary solutions of the wave equation in a medium with nonlinearity saturation, Radiophys. Quant. Electr. 16 (7) (1973) 783–789.

[37] J. Cuevas-Maraver, P. Kevrekidis, A. Vainchtein, H. Xu, Unifying perspective: Hamiltonian lattice traveling waves as discrete breathers and energy criteria for their stability, Phys. Rev. E 96 (2017) 032214.

[38] H. Xu, J. Cuevas-Maraver, P.G. Kevrekidis, A. Vainchtein, An energy-based stability criterion for solitary travelling waves in Hamiltonian lattices, Phil. Trans. R. Soc. A 376 (2117) (2018) 20170192.

[39] N. Triantafyllidis, S. Bardenhagen, On higher order gradient continuum theories in 1-d nonlinear elasticity. Derivation from and comparison to the corresponding discrete models, J. Elasticity 33 (3) (1993) 259–293.

[40] M.A. Collins, A quasicontinuum approximation for solitons in an atomic chain, Chem. Phys. Lett. 77 (1981) 342–347.

[41] P. Rosenau, Dynamics of nonlinear mass–spring chains near the continuum limit, Phys. Lett. A 118 (5) (1986) 222–227.
[42] L. Truskinovsky, A. Vainchtein, Quasicontinuum models of dynamic phase transitions, Contin. Mech. Thermodyn. 18 (1–2) (2006) 1–21.
[43] F. Theil, V.I. Levitas, A study of a hamiltonian model for martensitic phase transformations including microkinetic energy, Math. Mech. Solids 5 (3) (2000) 337–368.
[44] J. Giannoulis, A. Mielke, The nonlinear Schrödinger equation as a macroscopic limit for an oscillator chain with cubic nonlinearities, Nonlinearity 17 (2) (2003) 551–565.
[45] J.A.D. Wattis, Asymptotic approximation of discrete breather modes in two-dimensional lattices, in: Quodons in Mica, Springer, 2015, pp. 179–201.
[46] J.C. Eilbeck, R. Flesch, Calculation of families of solitary waves on discrete lattices, Phys. Lett. A 149 (4) (1990) 200–202.